Opto-Electronic Science

ISSN 2097-0382 CN 51-1800/O4

Solar cell-based hybrid energy harvesters towards sustainability

Tianxiao Xiao, Suo Tu, Suzhe Liang, Renjun Guo, Ting Tian and Peter Müller-Buschbaum

Citation: Xiao TX, Tu S, Liang SZ, Guo RJ, Tian T et al. Solar cell-based hybrid energy harvesters towards sustainability. *Opto-Electron Sci* **2**, 230011 (2023).

https://doi.org/10.29026/oes.2023.230011

Received: 17 May 2023; Accepted: 16 August 2023; Published online: 7 September 2023

Related articles

Giant magneto field effect in up-conversion amplified spontaneous emission via spatially extended states in organic-inorganic hybrid perovskites

Tangyao Shen, Jiajun Qin, Yujie Bai, Jia Zhang, Lei Shi, Xiaoyuan Hou, Jian Zi, Bin Hu

Opto-Electronic Advances 2022 **5**, 200051 doi: 10.29026/oea.2022.200051

Review of blue perovskite light emitting diodes with optimization strategies for perovskite film and device structure

Zongtao Li, Kai Cao, Jiasheng Li, Yong Tang, Xinrui Ding, Binhai Yu

Opto-Electronic Advances 2021 **4**, 200019 doi: 10.29026/oea.2021.200019

Charge carrier dynamics in different crystal phases of $CH_3NH_3PbI_3$ perovskite

Efthymis Serpetzoglou, Ioannis Konidakis, George Kourmoulakis, Ioanna Demeridou, Konstantinos Chatzimanolis, Christos Zervos, George Kioseoglou, Emmanuel Kymakis, Emmanuel Stratakis

Opto-Electronic Science 2022 **1**, 210005 doi: 10.29026/oes.2022.210005

Perovskite-transition metal dichalcogenides heterostructures: recent advances and future perspectives

Ahmed Elbanna, Ksenia Chaykun, Yulia Lekina, Yuanda Liu, Benny Febriansyah, Shuzhou Li, Jisheng Pan, Ze Xiang Shen, Jinghua Teng

Opto-Electronic Science 2022 **1**, 220006 doi: 10.29026/oes.2022.220006

More related article in Opto-Electron Journals Group website

Opto-Electronic Science

http://www.oejournal.org/oes

OE_Journal

Website

Opto-Electronic Science

Review

June 2023, Vol. 2, No. 6

DOI: 10.29026/oes.2023.230011

Solar cell-based hybrid energy harvesters towards sustainability

Tianxiao Xiao[1†], Suo Tu[1†], Suzhe Liang[1], Renjun Guo[1], Ting Tian[1] and Peter Müller-Buschbaum[1,2*]

Energy harvesting plays a crucial role in modern society. In the past years, solar energy, owing to its renewable, green, and infinite attributes, has attracted increasing attention across a broad range of applications from small-scale wearable electronics to large-scale energy powering. However, the utility of solar cells in providing a stable power supply for various electrical appliances in practical applications is restricted by weather conditions. To address this issue, researchers have made many efforts to integrate solar cells with other types of energy harvesters, thus developing hybrid energy harvesters (HEHs), which can harvest energy from the ambient environment *via* different working mechanisms. In this review, four categories of energy harvesters including solar cells, triboelectric nanogenerators (TENGs), piezoelectric nanogenerators (PENGs), and thermoelectric generators (TEGs) are introduced. In addition, we systematically summarize the recent progress in solar cell-based hybrid energy harvesters (SCHEHs) with a focus on their structure designs and the corresponding applications. Three hybridization designs through unique combinations of TENG, PENG, and TEG with solar cells are elaborated in detail. Finally, the main challenges and perspectives for the future development of SCHEHs are discussed.

Keywords: solar cell; hybrid energy harvesters; triboelectric nanogenerators; piezoelectric nanogenerators; thermoelectric generators

Xiao TX, Tu S, Liang SZ, Guo RJ, Tian T et al. Solar cell-based hybrid energy harvesters towards sustainability. *Opto-Electron Sci* **2**, 230011 (2023).

Introduction

The energy crisis in modern social life includes the increasingly urgent challenges of energy availability, affordability, and sustainability, which calls for a crucial transition from fossil fuels to cleaner and more renewable energy sources. Energy harvesting offers a multitude of advantages, such as sustainability, decreased reliance on external power sources, cost savings, environmental benefits, energy efficiency, versatility, and scalability. Thus, its crucial role in modern society is rooted in its potential capability to provide clean, decentralized, and dependable power solutions across a diverse range of applications, thereby contributing to a more sustainable future[1–3]. As traditional energy sources have limitations on reserves and environmental protection, renewable energy sources have become a focus of research and development efforts[4–7]. Renewable energy harvesters are considered devices, which can collect energy to generate

[1]Chair for Functional Materials, Department of Physics, TUM School of Natural Sciences, Technical University of Munich, James-Franck-Str. 1, 85748 Garching, Germany; [2]Heinz Maier-Leibniz Zentrum (MLZ), Technical University of Munich, Lichtenbergstraße 1, 85748 Garching, Germany.

[†]These authors contributed equally to this work.

*Correspondence: P. Müller-Buschbaum, E-mail: muellerb@ph.tum.de

Received: 17 May 2023; Accepted: 16 August 2023; Published online: 7 September 2023

electricity without harmful pollution from various environmental sources, such as wind[8,9], solar[10–13], human motions[14–18], water waves[19–21], and waste heat[22,23]. Among other counterparts, solar cells due to their numerous benefits, including low maintenance costs, low carbon footprints, and the abundant sources have been widely adopted as one of the most promising candidates[24–26]. In recent years, different types of solar cells have been fabricated for powering devices from small-scale electronics to large-scale networks and proved to be a reliable and sustainable energy harvesting technology, with the potential to significantly contribute to the global energy supply[27–34].

With the rapid development, the power conversion efficiency (PCE) and operational stability of solar cells have been extensively researched and continually improved[35–42]. However, only a high PCE cannot resolve the main issue of solar cells in providing a stable power supply due to the weather conditions[43]. It means that solar cells are highly dependent on the availability of the sunlight, and the performance is obviously affected by weather conditions such as cloudy or rainy days. To overcome this limitation, integrating solar cells with other kinds of energy harvesting techniques to offer more reliable, continuous and stable electricity is in high demand[44–48].

There are some newly arising energy harvesting systems, among which triboelectric nanogenerators (TENGs)[49,50], piezoelectric nanogenerators (PENGs)[51], and thermoelectric generators (TEGs)[52] are considered representative examples. Up to now, researchers have explored different approaches to hybridizing solar cells with these kinds of energy harvesters to create hybrid energy harvesters that can harness energy from the ambient environment *via* different working mechanisms[53–61]. Leveraging the complementary strengths of each energy harvesting technology, the hybridization of solar cells with TENGs, PENGs, and TEGs, has shown great potential in producing more stable power supplies for various applications (Fig. 1). Here, we summarize some progress of solar cell-based hybrid energy harvesters (SCHEHs) in recent years. This review begins with shortly introducing the working principles and achievements of solar cells, TENGs, PENGs and TEGs. Following that, the structural designs of SCHEHs are presented in detail with their functions and applications. At last, the challenges faced in the development of SCHEHs are discussed, and perspectives on future advancement are provided.

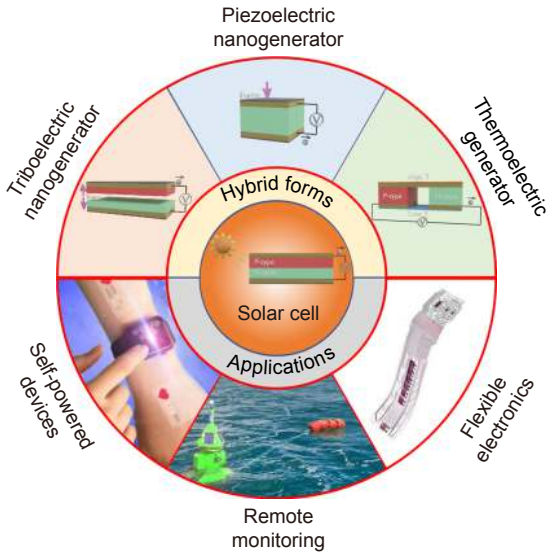

Fig. 1 | Outline illustration of the review of SCHEHs.

Energy harvesting systems

Photovoltaic effect-based energy harvester

Photovoltaic cells also known as solar cells are a type of energy harvester that can directly convert infinite solar energy into electricity by the photovoltaic effect, and the working principle of a typical solar cell is schematically shown in Fig. 2(a)[62]. When the solar cell is exposed to sunlight, the semiconductor in the solar cell absorbs the light energy, which creates electron-hole pairs. These charges are then transported to the electrodes, leading to a flow of electricity[63,64]. Here, the work function of the p-type semiconductor, n-type semiconductor, and electrodes is crucial for efficient charge transport and voltage generation. Therefore, achieving high energy conversion efficiency for a solar cell necessitates developing new materials and modifying their work function. The PCE of a solar cell is evaluated by

$$\eta\,(\%) = \frac{P_{\max}}{P_{\rm in}} = \frac{V_{\rm oc}J_{\rm sc}FF}{P_{\rm in}} \times 100\ , \qquad (1)$$

where $P_{\max}$ stands for the maximum output performance, $P_{\rm in}$ represents the input solar energy, $V_{\rm oc}$ is the open-circuit voltage, $J_{\rm sc}$ means the short-circuit current density, and *FF* is the fill factor. Here, the *FF*, which is defined as the ratio of the maximum power from the solar cell to the product of $V_{\rm oc}$ and $J_{\rm sc}$, is measured by the *I-V* scan.

Over the recent years, a large variety of solar cells based on diverse novel materials have been successfully fabricated *via* various deposition methods besides the traditionally well commercialized silicon solar cells and the rather well developed class of thin film solar cells.

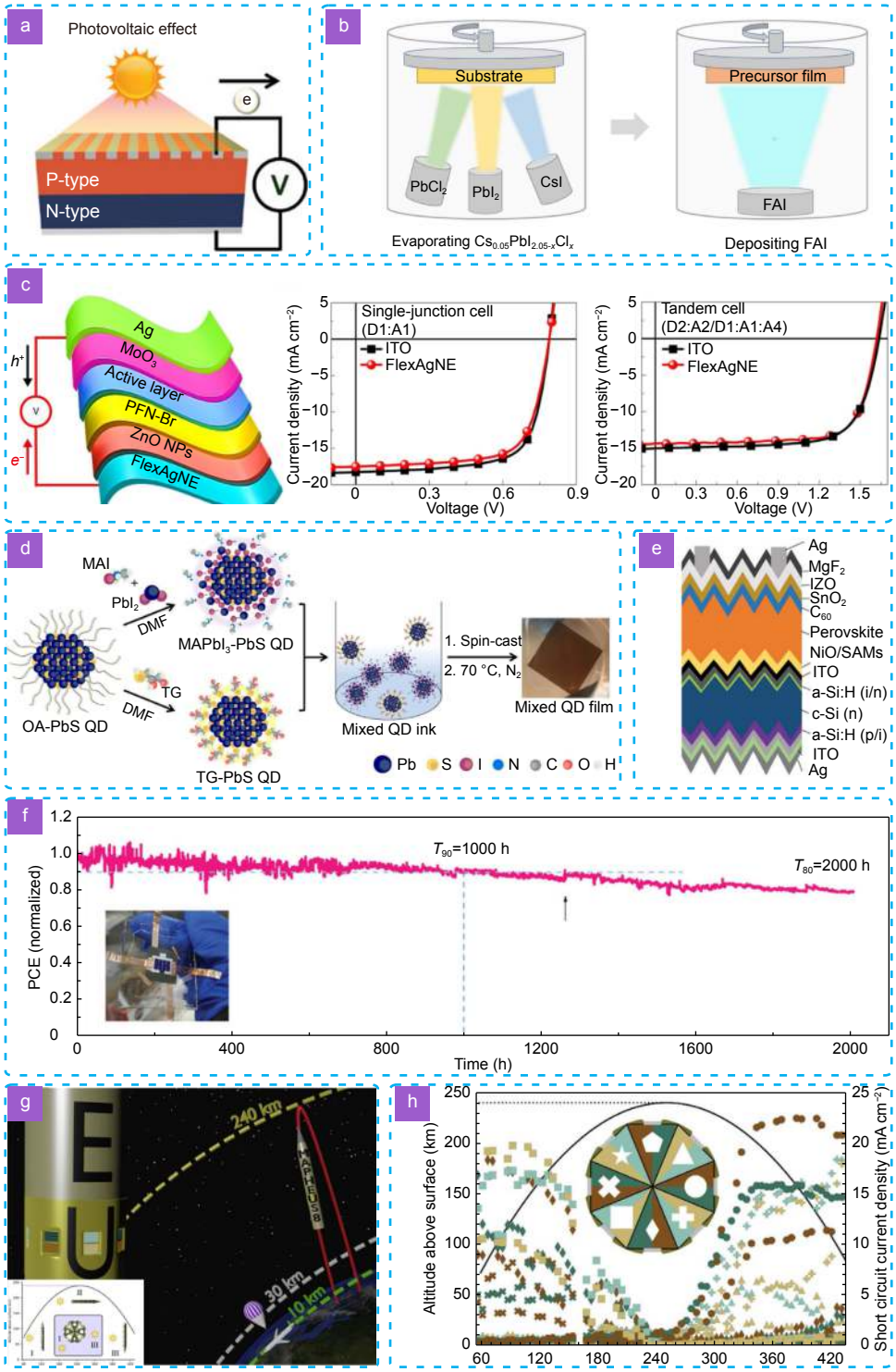

Fig. 2 | Photovoltaic effect-based energy harvester. (**a**) Schematic illustration of the photovoltaic effect-based energy harvester[44]. (**b**) Simplified scheme presenting the Cl-containing alloy-mediated sequential vacuum deposition approach[65]. (**c**) Schematic architecture of the flexible OSCs (left), *J-V* curves of a typical single-junction device (D1:A1) based on FlexAgNEs and ITO glass electrodes (middle), *J-V* curves of a typical tandem device (D2:A2/D1:A1:A4) based on FlexAgNEs and ITO electrodes (right)[66]. (**d**) Scheme of the solution ligand exchange process[67]. (**e**) Schematic diagram of perovskite/SHJ tandem solar cell[69]. (**f**) Maximum power point tracking of encapsulated tandem solar cells in air. Inset is the photograph of the encapsulated device[69]. (**g**) Schematic overview of the MAPHEUS-8 sounding rocket flight. Inset is the different illumination states[70]. (**h**) Scatter plot showing the J_{sc} evolution and flight-altitude (black line) during micro-gravity[70]. Figure reproduced with permission from: (a) ref.[44], Copyright © 2019 John Wiley and Sons; (b) ref.[65], Copyright © 2022 AAAS; (c) ref.[66], Copyright © 2019 Springer Nature; (d) ref.[67], under a Creative Commons Attribution 4.0 International License; (e, f) ref.[69], Copyright © 2023 John Wiley and Sons. (g, h) ref.[70], Copyright © 2020 Elsevier.

These promising next generation solar cells comprise perovskite solar cells (PSCs), organic solar cells (OSCs) and quantum dot solar cells (QDSCs). For example, Li et al. developed a chlorine (Cl)-alloy-mediated sequential vacuum deposition method for fabricating high-efficiency PSCs[65]. In this work, cesium iodide (CsI), lead iodide (PbI_2), and lead chloride ($PbCl_2$) were all evaporated to create a composite precursor film, which was followed by the precisely controlled deposition of formamidinium iodide (FAI) molecules (Fig. 2(b)). By utilizing this method, perovskite films with high crystallinity and homogeneity were obtained. The 1-cm^2 area PSC exhibited a champion PCE of 23.44% with the certified PCE of 22.6%. In case of OSCs, a new method for creating flexible transparent electrodes (FlexAgNEs) with high performance by using a water-based homogeneous suspension of silver nanowires (AgNWs) and poly(sodium 4-styrenesulfonate) (PSSNa) as a polyelectrolyte was presented by Sun and coauthors[66]. Their approach relied on the ionic electrostatic charge repulsion between the AgNWs originating from the preferred adsorption of PSSNa anions, which resulted in stable and uniform AgNWs suspensions. Combining the benefits of dry and wet methods and requiring no post-treatment, with FlexAgNEs the fabricated OSC devices exhibited high performance with single-junction cells achieving the best PCE of 13.15% and tandem achieving the best PCE of 16.55%, respectively (Fig. 2(c)). For QDSCs, a mixed-QD ink method, which could improve charge carrier extraction in the light harvesting layer of the QD solar cell was proposed by Yang et al. (Fig. 2(d))[67]. This mixed-QD ink method was based on the formation of a mixture of donor and acceptor QDs, and each of them retained its unique chemical properties when combined in the solution phase and finally formed into a film. At last, they utilized this mixed-QD ink method to fabricate the first mixed-QD ink solar cell and achieved a PCE of 10.4%, which was two times as high as the output performance of previously reported bulk heterojunction (BHJ) QD devices[68]. In addition, Luo et al. reported that the crystallization of wide-bandgap perovskite films could be well controlled *via* an anion-engineered additive method[69]. This anion-engineered additive method has multiple functions, which could improve the film crystallinity, decrease the trap density, and conformably deposit on industrially textured silicon (Si). The schematic diagram of the fabricated perovskite/Si heterojunction tandem solar cell is illustrated in Fig. 2(e), and a PCE of 28.6% (certified 27.9%, 1 cm^2) was obtained by this strategy. Moreover, a large-area PCE of 25.1% of the fabricated tandem solar cells for an area of 16 cm^2 was achieved, making it suitable for the scalable production of tandem solar cells. Furthermore, the wide-bandgap PSCs' operating stability was greatly enhanced by using this anion-engineered additive method, and the encapsulated tandem solar cells maintained more than 80% of their initial output performance after 2000 hours of operation under the 1-sun illumination in the ambient environment (Fig. 2(f)). Besides improving the PCE and working stability, real applications of solar cells have also been focused on by researchers in recent years. For example, Reb and coworkers reported an experiment, which was applied during a suborbital rocket flight (Fig. 2(g))[70]. In this work, the output characteristics of PSCs and OSCs were investigated under two different phases (i. strong solar irradiance; ii. faint scattered light from the Earth). As their results shown in Fig. 2(h), both PSCs and OSCs could reach their performance expectations when exposed to space conditions, which demonstrated their potential long-term applications in future satellite missions.

Triboelectric effect-based nanogenerator

The triboelectric effect-based nanogenerator called TENG is a newly arising technology that can convert ambient mechanical energy/triggering into electricity[71]. It originates from Maxwell's displacement current and is based on the coupling effect of triboelectrification and electrostatic induction during the periodic relative contact-separation motion of the surfaces of two materials[72]. The amount of electricity generated by TENG is strongly affected by the surface charge density, as illustrated in Fig. 3(a). The polarity of the surface charges, which is developed on materials, is determined by the triboelectric series, and these charges cause electric flow through the external circuit with specific potential differences[73]. The transfer process of a charge across the interface of two different materials appears when they come into contact, resulting in the generation of opposite charges on the surfaces of two materials. The relative motion of the two triboelectric materials causes the flow of electric charges between two electrodes after the generation of surface triboelectric charges in order to maintain the electrostatic equilibrium. The triboelectric potential V_{tri} can be expressed by the function

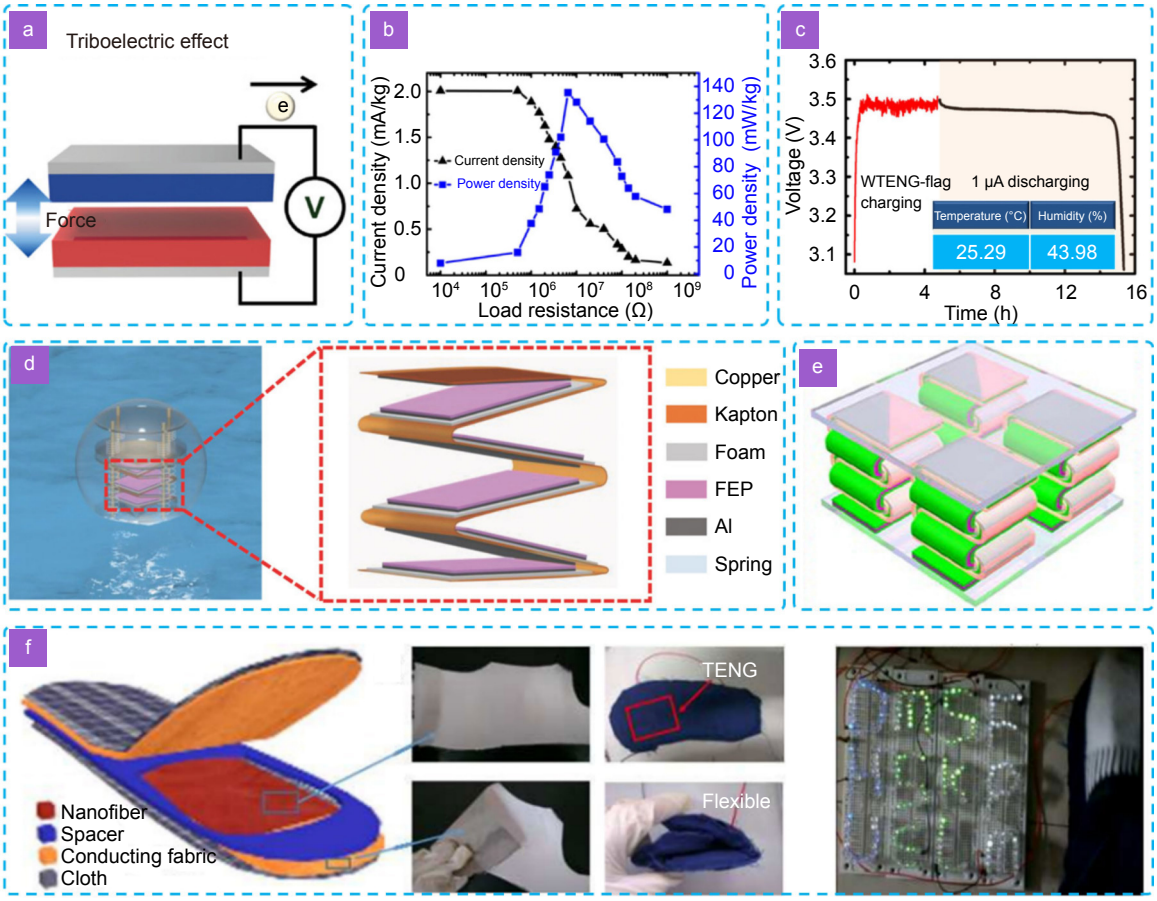

Fig. 3 | Triboelectric effect-based energy harvester. (**a**) Schematic illustration of the triboelectric effect-based nanogenerator[44]. (**b**) Variation of current and power of the TENG-flag with external load resistances and the output performances of the TENG-flag (the woven unit is 1.5 × 1.5 cm^2, and the degree of tightness is 1.09) at a 22 m s^{-1} wind speed[78]. (**c**) Voltage profiles of the button battery charged by TENG-flag and galvanostatically discharged at 1 μA[78]. (**d**) Schematic diagram of the spherical TENG with spring-assisted multilayered structure floating on water, and schematic representation enlarged structure for the zigzag multilayered TENG with five basic units[79]. (**e**) Schematic diagram of the folded elastic strip-based TENG[80]. (**f**) Schematic diagram (left) and photographs (middle) of the wearable all-fiber TENG, as well as hundreds of LEDs powered by the TENG[81]. Figure reproduced with permission from: (a) ref.[44], Copyright © 2019 John Wiley and Sons; (b, c) ref.[78], Copyright © 2016 American Chemical Society; (d) ref.[79], Copyright © 2018 John Wiley and Sons; (e) ref.[80], Copyright © 2015 American Chemical Society; (f) ref.[81], Copyright © 2015 Elsevier.

$$V_{\rm tri} = -\frac{\rho_{\rm tri} d}{\varepsilon_0}\,, \tag{2}$$

in which $\rho_{\rm tri}$ stands for the triboelectric charge density, d represents the gap distance between two triboelectric materials, and ε_0 is donated as the vacuum permittivity. The triboelectric current $I_{\rm tri}$ can be derived as

$$I_{\rm tri} = C_{\rm tri}\frac{\partial V_{\rm tri}}{\partial t} + V_{\rm tri}\frac{\partial C_{\rm tri}}{\partial t}\,, \tag{3}$$

where $C_{\rm tri}$ stands for the capacitance between two triboelectric materials and $V_{\rm tri}$ represents the generated triboelectric potential across the two electrodes. In contrast to the conventional electromagnetic generator (EMG) for mechanical energy harvesting, TENG has a high conversion efficiency at low-frequency ranges and has the advantages of a lightweight, easy fabrication, low costs, diverse choices of materials and high durability for long-term operations[74–76]. Four basic working modes of TENGs are known, including vertical contact-separation (CS) mode, lateral-sliding (LS) mode, single-electrode (SE) mode, and freestanding triboelectric-layer (FT) mode[77]. A typical CS-mode TENG consists of several layers, including two electrodes attached on the top and bottom as well as a pair of dielectric materials serving as triboelectric surfaces in between, such as polytetrafluoroethylene (PTFE), polyvinylidene difluoride (PVDF), polydimethylsiloxane (PDMS), and polyimide (PI), etc.

After TENG was first invented by Zhong Lin Wang in 2012, various kinds of TENG-based energy harvesters have been reported for harnessing the energy from mechanical motions. For example, Zhao et al. designed a

freestanding flag-type woven TENG for harvesting the wind energy from arbitrary directions by the interlaced interactions between Kapton film and a conductive cloth under wind-introduced fluttering of the flag[78]. At the wind speed of 22 m s^{-1}, their fabricated device could obtain the maximum output power peak density of 135 mW kg^{-1} at the matched resistance of 6.5 MΩ (Fig. 3(b)). Figure 3(c) shows the fabricated woven TENG successfully powered the wireless temperature and humidity sensor node to work for more than 10 h after the 4.8-hour charging process. Xiao and coauthors utilized the TENG technology to scavenge water wave energy with the spring-assisted multilayered structure[79]. In their study, the water waves were generated by using a series of wave pumps, which were controlled by a function generator, and each of their fabricated devices generated a maximum output power peak of 7.96 mW at 1.0 Hz water waves (Fig. 3(d)). Finally, the TENG array consisting of four optimized TENG spherical units connected in parallel was fabricated, which produced 15.97 mW and lighted up dozens of light-emitting diodes (LEDs). Meanwhile, the TENG technology is also widely utilized in harnessing the energy from human motions. Figure 3(e) shows that a folded elastic strip-based TENG for collecting the energy from human motions was proposed by Kang and coauthors[80]. With the optimization of strip width, deformation frequency, and amplitude, the output current, output voltage, and output power peak reached up to 55 μA, 840 V, and 7.33 mW, respectively. Huang et al. also fabricated a high-performance, wearable all-fiber TENG-based insole[81]. In this work, the surface of the nanofibers was roughened with secondary nanostructure to enhance the output performance. The maximum output voltage, output current, and output power peak of the TENG-based insole reached 210 V, 45 μA, and 2.1 mW, respectively. Thus, with the advantages of soft texture, good flexibility and lightweight, this TENG-based insole ensured a maximum comfort for the wearer, and it could convert mechanical energy to successfully light up 214 LEDs connected in series by the stepping force of the human (Fig. 3(f)).

Piezoelectric effect-based nanogenerator

Besides TENG, PENG is another widely used technology to convert mechanical energy into electricity[82]. The first PENG was presented by Zhong Lin Wang in 2006[51]. It was designed with a single zinc oxide (ZnO) NW bonded horizontally on a flexible substrate in 2008[83]. The piezoelectric effect is the property of certain materials to generate electricity in response to the applied mechanical stress or strain. The working mechanism of the PENG can be described as a transient flow of electrons driven by the piezopotential, which is schematically illustrated in Fig. 4(a). When the external force is applied to the PENG, the center of the cations and anions are relatively displaced, which results in a piezoelectric potential difference between the ends and creates a new balance state. Once electrodes are connected to the external circuit, the generated piezopotential will drive the electrons to flow across the external circuit to generate electricity. Upon releasing the pressure, the electrons will flow back to return to the initial state[84]. The piezoelectric polarization charge density $\rho_{\rm pie}$ can be expressed by

$$\rho_{\rm pie} = d_{\rm pie} X \,, \tag{4}$$

in which $\rho_{\rm pie}$ represents the polarization charge density, $d_{\rm pie}$ stands for the piezoelectric coefficient, and X is donated as the applied stress. Meanwhile, the electric field and potential can be calculated by the charge density

$$\nabla E = \frac{\rho_{\rm pie}}{\varepsilon} \,, \tag{5}$$

in which ∇E stands for the divergence of the electric field, and ε represents the permittivity. Therefore, the optimized design of the piezoelectric material and device structure are significant for the output performance of the PENG. A typical PENG consists of several layers, including a top electrode, a bottom electrode, and an insulator piezoelectric material layer, such as lead zirconate titanate (PZT), barium titanate ($BaTiO_3$), ZnO, and poly(vinylidene fluoride) (PVDF) as well as their copolymers.

Since the birth of the PENG concept, it has experienced a period of rapid development in the mechanical energy-harnessing research field. Xu et al. developed a flexible PENG based on multi-layer/multi-row alternators by integrated with vertical/horizontal ZnO NWs arrays. In their work, the ZnO NWs were strong enough to avoid mechanical deformation, and the entire PENG device demonstrated exceptional flexibility[85]. A maximum output voltage of 1.26 V, and a maximum output current of 28.8 nA was attained when the device was periodically bent and released. This maximum output voltage of 1.26 V was close to the voltage of conventional electrical devices (Fig. 4(b)). Meanwhile, a high-efficiency, lightweight, and large-area PZT thin-film-based PENG was successfully fabricated by Park and coauthors

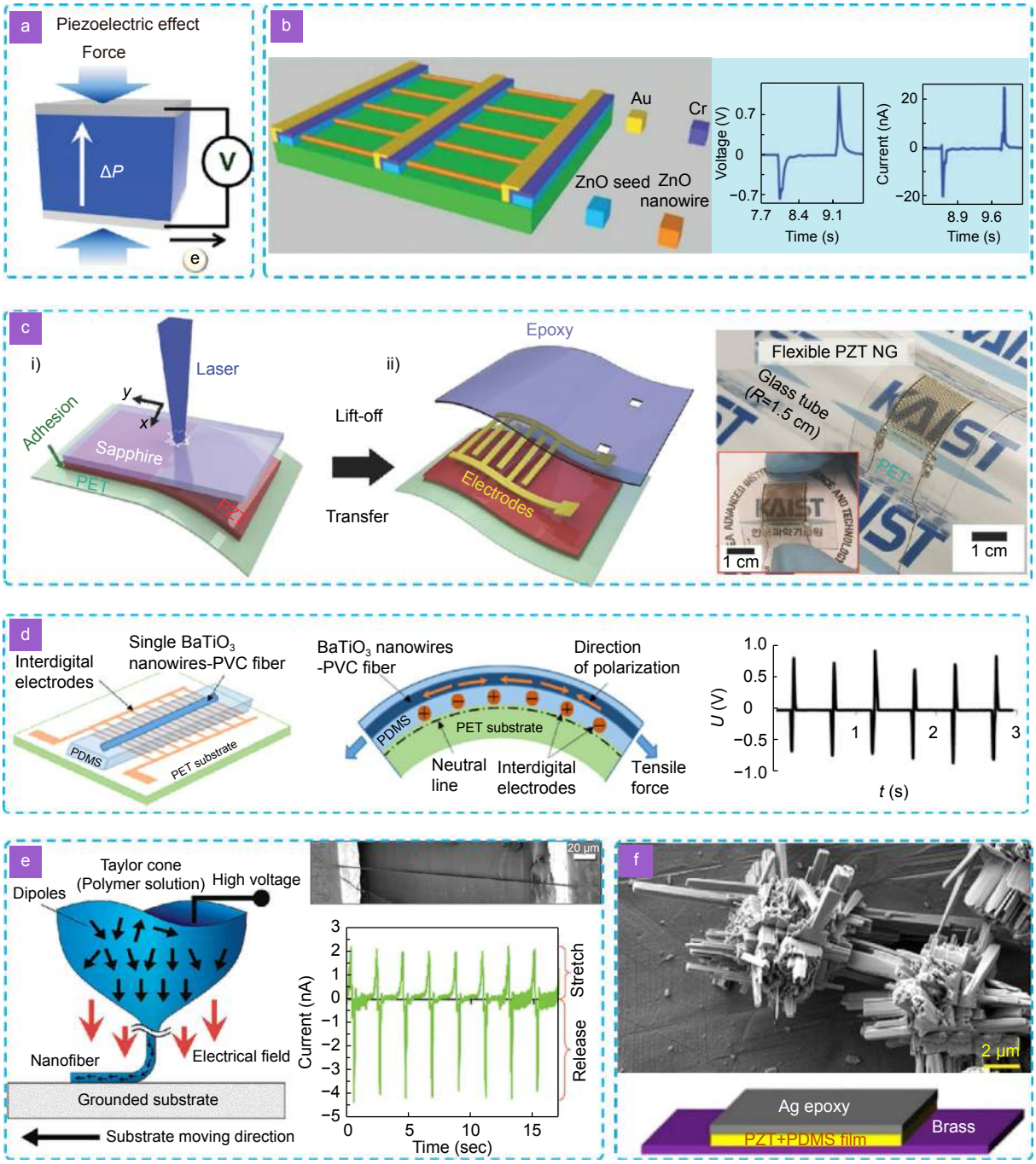

Fig. 4 | Piezoelectric effect-based energy harvester. (**a**) Schematic illustration of the piezoelectric effect-based nanogenerator[44]. (**b**) Schematic structure (left), output voltage (middle), and output current (right) of the lateral-nanowire-array integrated nanogenerator[85]. (**c**) Schematic diagram of the fabrication process (left) and the photograph (right) of a high-efficient, flexible, and large-area PZT thin film-based NG using the LLO method[86]. (**d**) Schematic images (left and middle) and the corresponding output voltage (right) of the flexible nanogenerator under the finger movement[87]. (**e**) Fabrication process (left), SEM image (top), and output current (bottom) of the piezoelectric PVDF nanogenerator[88]. (**f**) SEM image and the schematic structure of the PZT-PDMS energy harvester[89]. Figure reproduced with permission from: (a) ref.[44], Copyright © 2019 John Wiley and Sons; (b) ref.[85], Copyright © 2010 Springer Nature; (c) ref.[86], Copyright © 2014 John Wiley and Sons. (d) ref.[87], Copyright © 2015 Elsevier. (e) ref.[88], Copyright © 2010 American Chemical Society. (f) ref.[89], Copyright © 2018 American Chemical Society.

via utilizing the laser lift-off (LLO) process on the plastic substrate[86]. As shown in Fig. 4(c), by adopting this LLO method, the entire area of the PZT thin film could be transferred onto a flexible plastic substrate without causing any structural damage. During periodic bending-releasing motions, the output voltage of 200 V and the output current density of 150 μA cm^{-2} could be generated by the PZT-based PENG, respectively. Zhang et al. used the

spinning method to fabricate super flexible $BaTiO_3$-polyvinyl chloride (PVC) composite NWs for stretchable PENG devices[87]. In this work, the synthesis of $BaTiO_3$ nanowires with <001> orientation was accomplished by a topochemical method. The reported output voltage and output current could reach 0.9 V and 10.5 nA respectively under the finger movement (Fig. 4(d)). Besides $BiTiO_3$, the spinning electrospinning method combining direct-write, mechanical stretching, and in-situ electrical poling was also applied on PVDF NWs to successfully fabricate a flexible PENG by Chang and coauthors[88]. In their work, dipoles in the PVDF NW crystal were naturally aligned by the strong electric fields and stretching forces from the electrospinning process, leading to the transformation of the nonpolar α-phase into the polar β-phase. Under periodic long-term reliability tests, a single PVDF NW-based PENG's output performance was relatively stable without obvious degradation, demonstrating the stability of their fabricated PENG (Fig. 4(e)). In Fig. 4(f), Zhang and coauthors designed a flexible PENG by bonding the PZT NWs with a PDMS polymer[89]. In their work, PZT NWs with a diameter of 100 nm and a length of 6 μm were synthesized *via* a facile hydrothermal process. The output voltage of 2.7 V, and the output power peak density of 51.8 μW cm^{-3} with a matched external load resistance of 2 MΩ could be achieved at the frequency of 25.2 Hz. This PZT-based PENG could output 8 times more power than previously reported $BaTiO_3$-based PENG.

Thermoelectric effect-based generator

Unlike the piezoelectric effect, which is a property of specific materials that generate an electric charge when subjected to mechanical stress or strain, the thermoelectric effect is a phenomenon where the application of a temperature gradient across specific materials leads to the generation of an electric voltage. It is based on the Seebeck effect, which establishes that when there exists a temperature difference between two ends of a material with different electrical conductivity, an electric potential is induced. This effect is reversible, enabling the creation of a temperature difference by passing an electric current through the material, known as the Peltier effect[90,91]. Figure 5(a) shows the direct and efficient conversion between thermal energy and electricity based on the Seebeck effect. It is hence considered a sustainable alternative towards the re-utilization of heat sources for future energy supply[92]. A thermoelectric material is commonly quantified by using the nondimensional figure-of-merit (ZT) of the thermoelectric material

$$ZT = \frac{S^2\sigma(T_{\rm hot} - T_{\rm cold})}{\kappa}, \tag{6}$$

in which S stands for the material-specific Seebeck coefficient, σ represents the electrical conductivity, κ is denoted as the thermal conductivity (including electronic $\kappa_{\rm el}$ and phononic $\kappa_{\rm ph}$ contributions), $T_{\rm hot}$ (K) is the hot-side temperature, and $T_{\rm cold}$ (K) is the cold-side temperature[93]. An ideal TEG efficiency, $\eta_{\rm TEG}$, can be written as a function of the temperatures and the ZT, which is illustrated as follows[94]

$$\eta_{\rm TEG} = \frac{T_{\rm hot} - T_{\rm cold}}{T_{\rm hot}} \frac{\sqrt{1+ZT}-1}{\sqrt{1+ZT}+T_{\rm cold}/T_{\rm hot}}. \tag{7}$$

In contrast to conventional heat engines utilizing the working fluid to convert thermal energy to kinetic energy, the TEG, which can directly convert heat energy into electricity by utilizing the unique "working fluid" of charge carriers (holes or electrons, shown in Fig. 5(b)), has emerged as another environmental-friendly solution with merits of zero-emission, no circulating liquid or gas, no moving parts, silence, scalability and durability in recent years.

Currently, a major driving force for TEG's application is in automotive and industrial waste heat recovery to achieve resource reuse[95]. Because the efficiency of automobiles is less than 30%, and more than 2/3 of energy is directly dissipated as waste heat to the environment through the exhaust pipe and the radiator[96]. For example, in a recent work, Honda company demonstrated a proof-of-concept prototype (Figure 5(c)) with a maximum of approximately 500 W for automotive waste heat recovery[97]. They used a simple design of a thin flat rectangular box with TEGs placed on the top and bottom surfaces of the exhaust pipe and claimed a fuel consumption reduction of around 3%. Iezzi et al. demonstrated a flexible planar TEG, which could extract heat from industrial heat pipes to power a wireless sensor network[98]. The proposed module of 420 Ag/nickel (Ni) thermocouples were prepared on a flexible substrate in order to match the cylindrical form of the pipe (Fig. 5(d)). Their TEG generated an output power of 308 μW at the temperature gradient of 127 K. Meanwhile, TEGs that use thermal energy generated by the human body as a constant heat source are also well-appropriate for a wide variety of wearable and biomedical electronics within the nW to mW power range due to permanent direct current (DC)

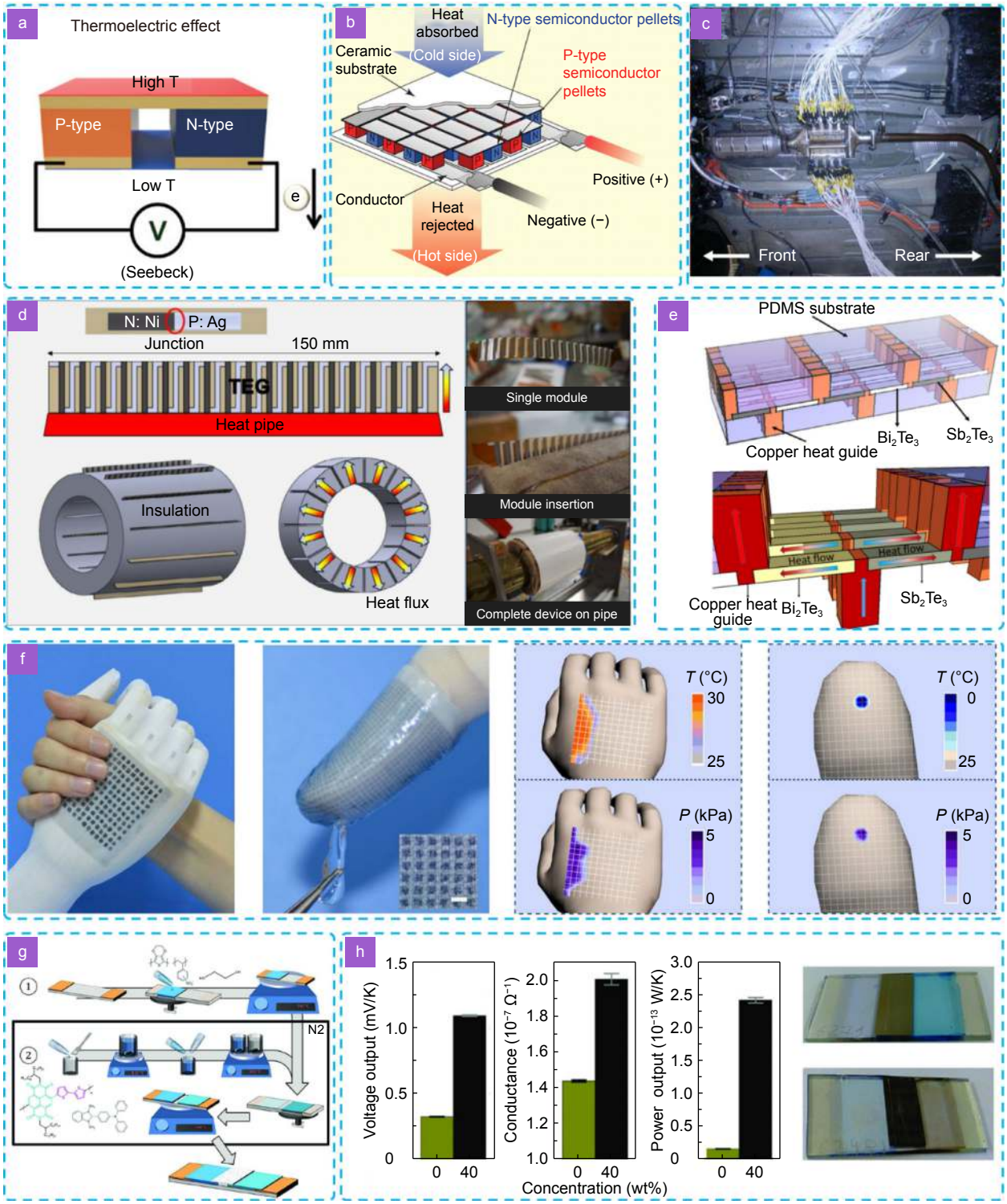

Fig. 5 | Thermoelectric effect-based energy harvester. (**a**) Schematic illustration of the thermoelectric effect-based generator[44]. (**b**) Practical TE generators connecting large numbers of junctions in series to increase operating voltage and spread heat flow[23]. (**c**) Honda prototype TEG exhaust heat recovery system[97]. (**d**) Schematic illustration (left) and photographs (right) of the complete TEG device on pipe[98]. (**e**) Structure of the proposed lateral Y type FTEGs[101]. (**f**) Practical applications of the fabricated dual-functional sensor as electronic skins[103]. (**g**) Sketch of the sample preparation of a solution-processable all-polymer TEG[110]. (**h**) Performances (left), as well as photographs of the undoped (top) and 40 wt% doped (bottom) thin-film TEGs[110]. Figure reproduced with permission from: (a) ref.[44], Copyright © 2019 John Wiley and Sons; (b) ref.[23], Copyright © 2008 AAAS; (c) ref.[97], Copyright © 2016 Elsevier; (d) ref.[98], Copyright © 2017 Elsevier; (e) ref.[101], Copyright © 2018 Elsevier. (f) ref.[103], under a Creative Commons Attribution 4.0 International License. (g, h) ref.[110], Copyright © 2020 John Wiley and Sons.

output[99,100]. Trung et al. fabricated a flexible TEG by using an electrochemical deposition process to synthesize thermoelectric materials including bismuth telluride (Bi_2Te_3) and antimony telluride (Sb_2Te_3)[101]. In their work, a novel idea of lateral Y-type TEG instead of conventional vertical π-type TEG was proposed to enhance the output performance of temperature energy harvesting. Fig. 5(e) shows that with the temperature difference of 22 °C between the human body and the ambient environment, the fabricated TEG device could generate approximately 3 mW cm^{-2} of output power density. Organic thermoelectrics exhibit potential for wearable heating and cooling devices, and near-room-temperature energy generation[102]. Zhang and coworkers reported a flexible temperature-pressure dual-parameter sensor by casting conductive polymer poly(3,4-ethylenedioxythiophene): poly(styrenesulfonate) (PEDOT:PSS) on a microstructured polyurethane (PU) foam *via* a dip coating method[103]. This dual-functional sensor could be self-powered by a thermovoltage during the temperature sensing without any other external power supply. The maximum power of 80 μW and the output voltage of 220 mV could be achieved at a temperature difference of 100 K. The practical application of the dual-functional sensor as electronic skins was further presented in this work, as shown in Fig. 5(f). However, organic thermoelectrics typically suffer from low electrical conductivity and Seebeck coefficient, leading to a poor power factor. A lot of efforts have been devoted to uncoupling the trade-off relationship between them and then greatly enhancing them simultaneously[104]. Several effective approaches were reported to improve the conversion efficiency of organic thermoelectrics, including organic solvent treatment[93,105–106], ionic liquids treatment[92,107], salt solution treatment[108], and solution doping treatment[109]. To construct highly efficient devices, the utilization of appropriate thermoelectric materials, encompassing both n-type and p-type varieties, is imperative. Kluge and coworkers reported a novel solution-processable TEG[110]. In this work, the TEG incorporated a high-mobility n-type polymer called poly[[N,N-bis(2-octyldodecyl)-naphthalene-1,4,5,8-bis(dicarboximide)-2,6-diyl]-alt-5,5-(2,2-bithiophene)] (P(NDI2OD-T2)), along with the widely studied p-type polymer blend, PEDOT:PSS, forming a thin-film structure (Fig. 5(g)). This TEG demonstrated a competitive power output of 2.4×10^{-13} W cm^{-2} K^{-1} (Fig. 5(h)) and offered the advantage of facile scalability to fully flexible devices through techniques such as printing and roll-to-roll processing.

Structures, outputs, and applications of SCHEHs

SCHEHs based on solar cell and triboelectric nanogenerator (SC-TENG)

With the integration of solar cells and TENGs, the emergence of SC-TENGs enables energy harvesting systems to be more effective even when no sunlight appears and thus achieves all-weather sustainable energy harnessing[111]. Therefore, SC-TENG becomes one of the hottest topics in the research field of SCHEHs. For example, Liu et al. designed an SC-TENG by integrating a solar cell with a TENG *via* a mutual electrode[112]. This SC-TENG could harvest both types of energies from sunlight and raindrops. In the configuration of this SC-TENG, a single-electrode mode TENG with a PDMS film as the triboelectric layer on the Si solar cell was utilized to harvest the energy from raindrops, as shown in Fig. 6(a). The imprinted structure on the top surface of the PDMS film effectively increased the real contact area between the TENG and raindrops, which improved the outputs of the TENG component. An output voltage peak of 2.14 V and an output current peak of 33.0 nA were achieved. The sunlight harvesting was realized by a Si-based solar cell with a PCE of 13.6%, in which an imprinted PEDOT:PSS film was used as the electrode for both, the Si-based solar cell and the TENG. In 2021, Zhao and coworkers established a two-electrode TENG by connecting the top Ag and the bottom aluminum (Al) electrodes (Fig. 6(b))[113]. This Al electrode introduced a build-in electric field that induced a charge redistribution in the whole Si/TENG tandem hybrid device, leading to a higher output performance. This tandem hybrid device achieved a champion PCE of 22.04% under one sun illumination, and a maximum output power peak of 147 μW with the output voltage of 37.19 V and the output current of 7.59 μA under one raindrop. These two SC-TENGs demonstrated an effective approach to harvest energy from the environment in different weather conditions. Besides Si-based solar cells, TENGs were also successfully utilized to assist OSC and dye-sensitized solar cell (DSSC) to harvest multiple energies. As shown in Fig. 6(c), Ren et al. proposed a flexible common-electrode SC-TENG based on a single-electrode mode TENG and an OSC[114]. The ITO film in this work was regarded as the anode of the OSC and the electrode of the TENG.

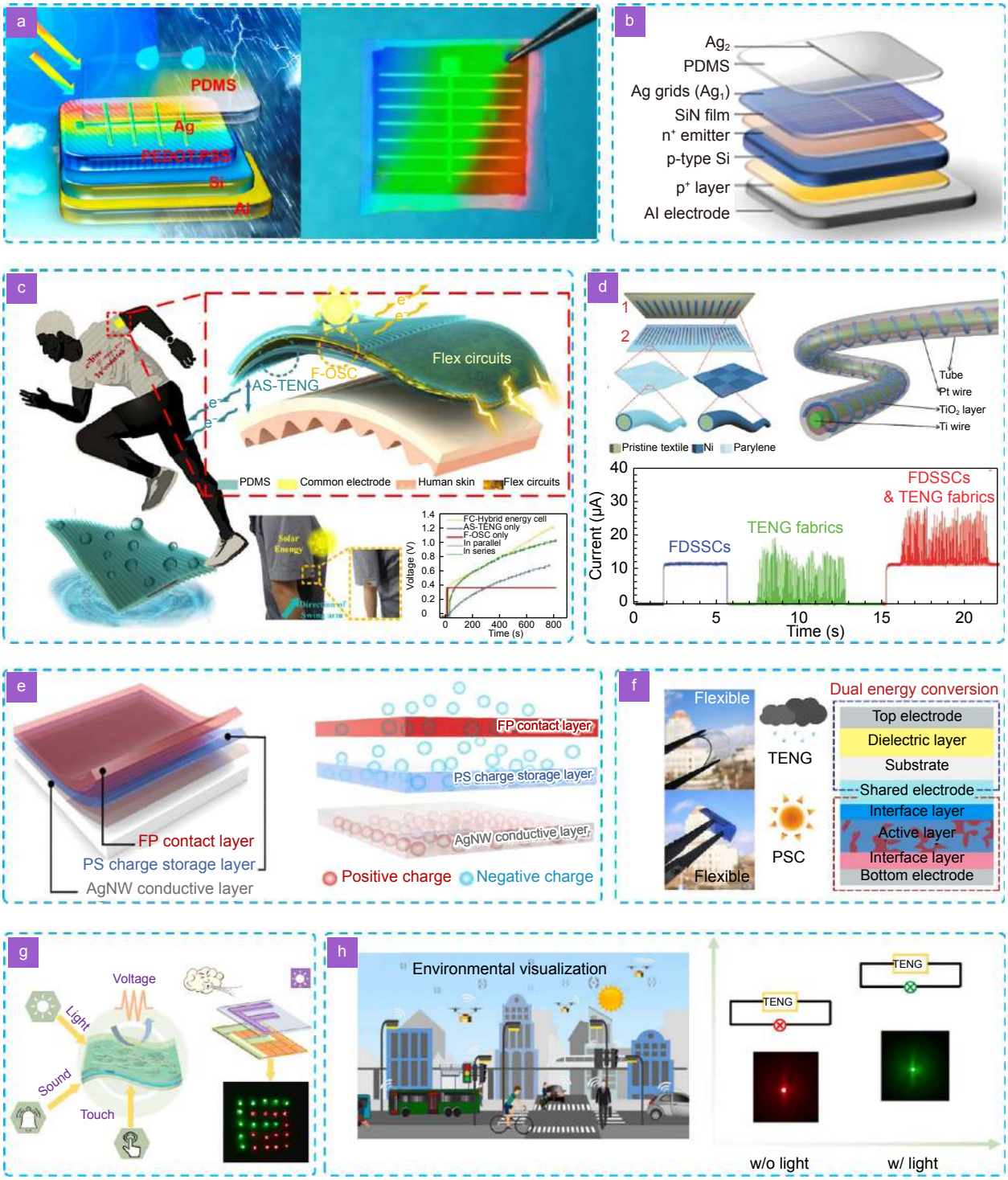

Fig. 6 | SCHEHs based on solar cell and triboelectric nanogenerator. (**a**) Schematic illustration and the photograph of the hybrid energy harvester[112]. (**b**) Architecture of the hybrid TENG/Si tandem solar cell[113]. (**c**) Schematic illustration of the flexible hybrid energy harvesting system[114]. (**d**) Scheme of the configuration of the TENG fabrics and the fiber-shaped dye-sensitized solar cell (top), as well as output current of the hybrid energy-harvesting device[115]. (**e**) Schematic illustration (left) and the working principle (right) of the raindrop-solar hybrid energy harvester with embedded charge-storage layer[116]. (**f**) Photographs and the schematic illustration of the synergistic solar and raindrop hybrid energy harvester[117]. (**g**) Schematic diagram of the multifunctional hybrid device[118]. (**h**) Schematic illustration of the self-powered environmental visualized system (left), and alterable colored LED showing different light at different environment (right)[118]. Figure reproduced with permission from: (a) ref.[112], Copyright © 2018 American Chemical Society; (b) ref.[113], Copyright © 2021 Elsevier; (c) ref.[114], Copyright © 2020 Elsevier. (d) ref.[115], Copyright © 2016 John Wiley and Sons. (e) ref.[116], Copyright © 2022 Elsevier; (f) ref.[117], Copyright © 2022 Elsevier; (g, h) ref.[118], Copyright © 2021 Elsevier.

By introducing the groove-shaped micro/nanostructured haze thin film (GHF) into the SC-TENG, this flexible hybrid device was able to be well encapsulated to realize characteristics of dust-proof and self-cleaning. Additionally, Pu and coworkers integrated fabric TENGs and fiber-shaped DSSC (FDSSC) to design a whole textile-based SC-TENG energy harvesting system (Fig. 6(d))[115]. Both, the energy from human motions and solar light could be harvested by their hybrid device. The output performance of the TENG fabrics was further optimized by reducing the segment size, achieving an output power peak density of 3.2 W m^{-2} at the sliding speed of 0.75 m s^{-1}. By connecting the TENG fabrics and the FDSSC pack in parallel, this hybrid power textile could sum the outputs from both components. Kim et al. reported an all-aerosol-sprayed transparent TENG with the introduction of a transparent polystyrene (PS) charge-storage layer between the AgNW conductive layer and fluoropolymer (FP) contact layer for fabricating an SC-TENG system[116]. Unlike the SC-TENG without the PS charge-storage layer, the PS charge-storage layer in this SC-TENG could capture the migrating charges from the FP contact layer at its aromatic ring (Fig. 6(e)). When the counter layer contacted with the FP contact layer, surface charges on the FP contact layer and trapped charges in the PS charge-storage layer synergistically induced more positive charges in the counter layer, which resulted in the enhanced magnitude of the electric current from the AgNW layer to the ground. As the periodic contact and separation motions between the counter layer and contact layer, the generated electricity increased until the PS charge-storage layer was fully charged with the migrating charges from the FP contact layer. With water droplets, the highest electrical outputs of 5.0 V and 18 μA could be obtained by the fabricated SC-TENG system. For another example, Liu et al. fabricated a high-performance SC-TENG *via* a monolithic design for window-integrated applications (Fig. 6(f))[117]. The new function of water drop power conversion was endowed to the SC-TENG in their work. A maximum PCE of 12.7% (at 1-sun illumination), electrical output power peak of 2.62 W m^{-2} with an output voltage of 100 V, an output current of 120 μA, and transfer charges of 60 nC were achieved. Moreover, the fabricated SC-TENG could sustain the plant growth due to the controlled transmission and ambient temperature, which highlighted the great potential for energy-wise window-integrated applications of their work. Figure 6(g) shows that Liu and coworkers developed a one-structure-layer multifunctional stretchable PDMS/mxenes-based SC-TENG that could simultaneously detect changed environments and efficiently convert both mechanical and solar energies into electricity[118]. In this work, outstanding output voltage of 453 V, output current of 131 μA, and a PCE of 19.4% were attained by the fabricated SC-TENG, which could sufficiently compensate for the little effect on the energy loss of each component. Finally, the ability to distinguish different signals from the surroundings of this SC-TENG was demonstrated, which exhibited its huge potential for environmental monitoring (Fig. 6(h)).

SCHEHs based on solar cell and piezoelectric nanogenerator (SC-PENG)

In 2009, Xu and coauthors reported the first SC-PENG for scavenging solar and mechanical energies by building a DSSC on the top surface of ZnO NWs. The design and structure of their SC-PENG are shown in Fig. 7(a). With the operation of PENG, the J_{sc} of the SC-PENG could be slightly increased by 1.5 μA cm^{-2} to 45.5 μA cm^{-2} in this work[119]. Followed by another work from this group in 2011, a fully integrated solid-state compact SC-PENG consisting of convoluted ZnO NWs for harvesting diverse types of energies in one device was developed (Fig. 7(b))[120]. Compared to their first work, the liquid electrolyte was replaced by a solid electrolyte, which could avoid the possibility of solvent leakage and evaporation of the device. Both, the solar cell component and the PENG component of this compact SC-PENG could work independently and conjunctionally. When applying full sunlight (1-sun illumination) and ultrasonic waves of 41 kHz on the fabricated SC-PENG, the output power density of the SC-PENG achieved 34.5 μW cm^{-2} at the V_{oc} of 0.243 V and the J_{sc} of 141 μA cm^{-2}. A 6% enhancement (2 μW cm^{-2}) of the output power density was obtained after the addition of the PENG component. Moreover, Ahmed et al. developed a tree-shaped SC-PENG by using flexible sheets of photovoltaic and piezoelectric films (Fig. 7(c))[121]. Besides the electricity generation, a custom-made circuit for this integrated SC-PENG energy harvester was designed to convert alternating current (AC) signals generated by the PENG component to DC signals. At the wind speeds of 7–8 m s^{-1}, an SC-PENG consisting of 10 piezo films and 3 photovoltaic films could generate a maximum output voltage of 5.071 V, a maximum output current of 1.281 mA, and a

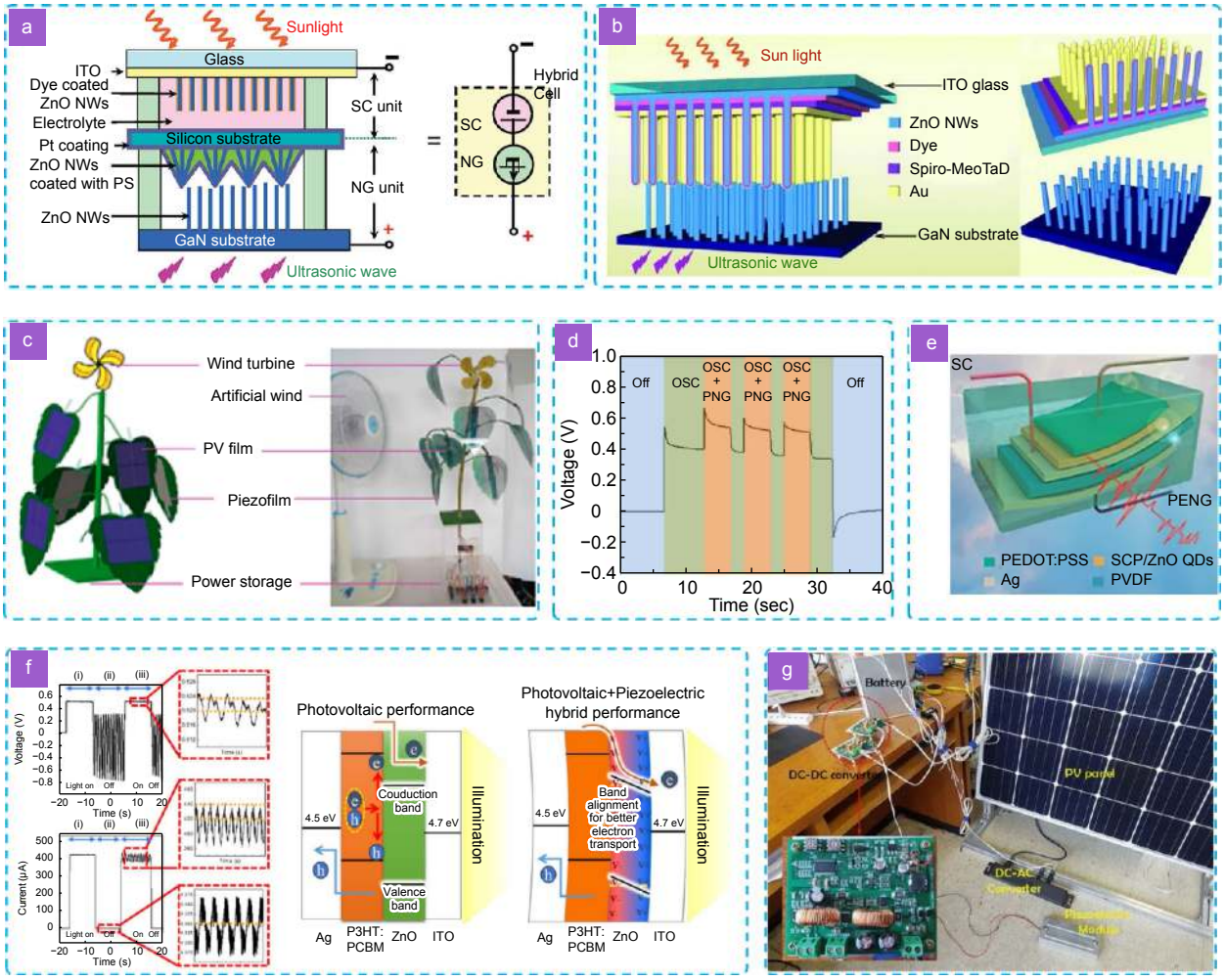

Fig. 7 | SCHEHs based on solar cell and piezoelectric nanogenerator. (**a**) Schematic structure of a serially integrated hybrid cell[119]. (**b**) Schematic illustration of a compact hybrid cell[120]. (**c**) Schematic illustration (left) and the photograph (right) of the tree shaped hybrid nanogenerator[121]. (**d**) Output voltage of the hybrid cell when the pressure is applied periodically at an interval of 3.0 s for an extended period of 1.0 s[122]. (**e**) Schematic illustration of a composite photovoltaic/PENG film[123]. (**f**) Output performance (left) and schematic illustration (middle and right) of the hybrid device with the bending instrument[124]. (**g**) Experimental configuration of the parallel hybrid power system[125]. Figure reproduced with permission from: (a) ref.[119], Copyright © 2009 American Chemical Society; (b) ref.[120], Copyright © 2011 John Wiley and Sons; (c) ref.[121], under a Creative Commons Attribution 4.0 International License; (d) ref.[122], Copyright © 2015 Elsevier; (e) ref.[123], Copyright © 2020 Springer Nature; (f) ref.[124], Copyright © 2022 Springer Nature; (g) ref.[125], Copyright © 2021 Springer Nature.

maximum output power of 3.42 mW with the matched external load resistance of 5 kΩ. Within only 15 seconds, a 1000 μF capacitor could be charged to power LEDs by the fabricated SC-PENG. Yoon and coauthors proposed another high-performance SC-PENG based on an OPV device and a DC PENG[122]. The output performance of the as-fabricated SC-PENG in this work is shown in Fig. 7(d). First, the output voltage was maintained at 0 V without any light and mechanical pressure. Second, when the light was lit up, the output voltage dramatically increased and then kept at 0.4 V owing to the OPV device contribution. After that, the periodic mechanical pressure was applied to the SC-PENG, and the output voltage was improved to a maximum value of 0.71 V with the operation of the DC PENG unit. For another example, Liu et al. fabricated a flexible, facile, and stable SC-PENG by spin coating at room temperature in the ambient air condition (Fig. 7(e))[123]. In this work, they found that the piezoelectric properties had no harmful effect after being coated by the solar cell unit. Under 1-sun illumination and the mechanical force of 26.1 N, the SC-PENG exhibited the output power density of 0.97 mW cm^{-3} at the matched load resistance of 600 kΩ. The practical application of their fabricated SC-PENG had been verified by using it to charge a capacitor with the capacitance of 33 μF to 3.6 V in 60 seconds. Besides the

research on the hybrid device itself, Kim and coworkers proposed a rationally designed hybrid-bending instrument for reliably evaluating the output performance of the SC-PENG in harvesting solar and mechanical energy sources simultaneously (Fig. 7(f))[124]. In this work, by using the designed bending instrument, the output performance of the SC-TENG could be reliably evaluated without height change, avoiding variations in photovoltaic electricity under mechanical bending. Furthermore, for more efficient energy harvesting of the SC-PENG, a hybrid parallel power control scheme was presented by Lee (Fig. 7(g))[125]. In this scheme, a buck-boost DC-DC converter with an additional split current path was designed to assume control over the battery in any condition by detecting the battery charging and discharging current. Using this proposed scheme, stable battery management for the hybrid parallel power system consisting of the solar cell and the PENG could be implemented.

SCHEHs based on solar cell and thermoelectric generator (SC-TEG)

In comparison to mechanical energy harvesters such as TENG or PENG, TEGs are integrated with solar cells due to the natural heat generation that occurs during the collection of solar energy. Some pioneering studies which date back to the 20th century have been researched[126]. Splitting SC-TEG and integrated SC-TEG are the two most common technologies for the fabrication of SC-TEGs[127]. For example, a splitting SC-TEG, which integrated a solar cell and a TEG to harvest solar energy from a wide spectral range was proposed by Li and coauthors[128]. As shown in Fig. 8(a), the incident sunlight was split using the solar spectrum splitter for both solar cell and TEG. To compensate for the discontinuous nature of solar radiation, a thermal energy storage unit was added to their SC-TEG device. For this SC-TEG, during the off-peak time, the cooling load was supplied by the ambient resources, and the surplus electricity would be stored in the form of high-grade cold in a deep freezer. Conversely, during the peak time, the stored cold was utilized to supercool solar cell and TEG to amplify their output power. Ju et al. presented guidelines when designing and optimizing a splitting SC-TEG[127]. It was found that the optimized cut-off wavelengths were nearly identical (Fig. 8(b)). Furthermore, the maximum efficiency of the splitting SC-TEG increased from 26.62% to 27.49% with the heat transfer coefficient increasing from 3000 to 4500 W m^{-2} K^{-1} when compared to the only solar cell unit (Fig. 8(c)). As an example of the integrated SC-TEG, Deng et al. developed an integrated design of a solar-driven SC-TEG that consisted of a Si thin-film solar cell module, a TEG module and a heat collector, in which Cu foil was fabricated to a bowl shape in order to conduct heat to the TEG module (Fig. 8(d))[129]. Their findings showed that the integrated design improved the synchronous performance of both solar cell and TEG. Here, the heat flux on the hot side of the TEG integrated into this SC-TEG hybrid system was more than tenfold. The total generated power was 393 mW, which was twice as much as that of the single solar cell module. In addition, Xu and coworkers fabricated a perovskite-based SC-TEG by integrating the PSC on the titanium dioxide/zirconium dioxide/carbon (TiO_2/ZrO_2/carbon) structure and the TEG, as shown in Fig. 8(e)[130]. The fabricated SC-TEG delivered a V_{oc} of 1.29 V, a J_{sc} of 22.80 mA cm^{-2}, a *FF* of 0.69, and a PCE of 20.3% with the assistance of 9 pieces of TEGs. Compared to the performance of the single PSC, a 48.3% improvement on the V_{oc} was achieved without any sacrifice of the J_{sc} after the integration. Moreover, a Cd-free $CuInGaSe_2$ (CIGS) based SC-TEG with ZnO NWs was proposed by Hsueh and coauthors[131]. The schematic cross-section of this SC-TEG is shown in Fig. 8(f), which could simultaneously generate solar cell-based and thermoelectric-based electricity. In their study, the J_{sc} was increased to 1.5 mA cm^{-2} by the addition of ZnO NWs. Finally, the output performance of their fabricated SC-TEG showed that the V_{oc} increased from 0.64 V to 0.84 V, the J_{sc} climbed from 36.21 mA cm^{-2} to 38.55 mA cm^{-2}, and the PCE was improved from 16.5% to 22.02%. Liu et al. developed a carbon counter electrodes based SC-TEG with excellent thermal endurance and photo-electric conversion (Fig. 8(g))[132]. When using the ice bath to cool the cold side of the TEG component, the total PCE of the SC-TEG boosted from 9.88% (only solar cell component) to 22.2% (both solar cell and TEG), and the maximum output power density of 22.2 mW cm^{-2} with the maximum V_{oc} of 1.87 V could be generated under AM 1.5G illumination. Another novel Monte Carlo-Finite Difference Time Domain (MC-FDTD) coupled method for improving the uniformity of the absorbed irradiance distribution by using various dimensional nanostructures was proposed by Zhou and coworkers[133]. According to their study, the presence of moth-eye nanostructures could improve the overall conversion efficiency of the SC-TEG. Jurado et al. for the first time reported an all organic flexible SC-TEG[134]. In this

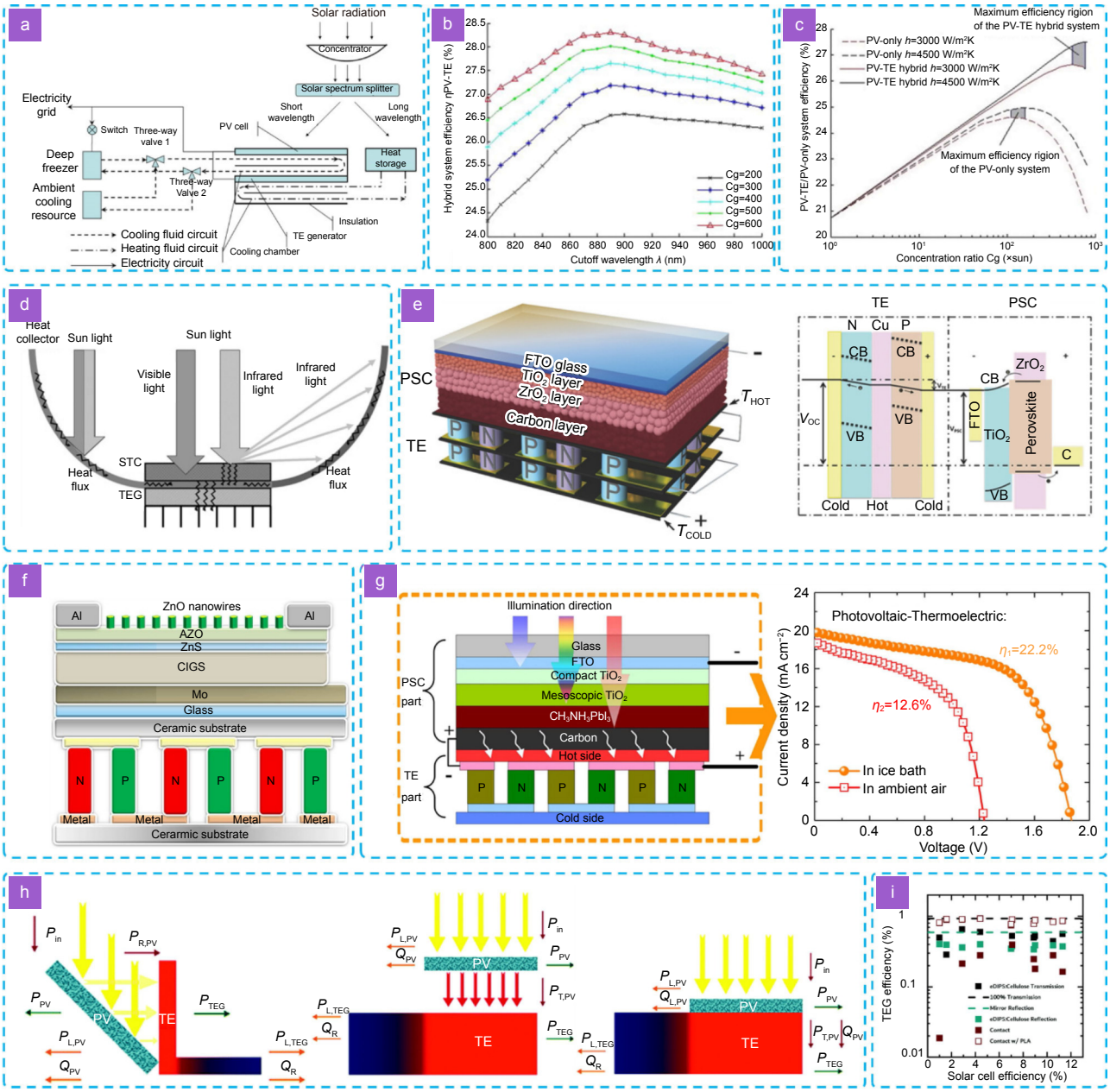

Fig. 8 | SCHEHs based on solar cell and thermoelectric generator. (**a**) Schematic of the PV-TE hybrid power system[128]. (**b**) Hybrid system efficiency vs. cutoff wavelength for different concentration ratio (h = 10000 W/m^2 K^{-1})[127]. (**c**) Comparison of the efficiency between the PV-only system and the PV-TE hybrid system[127]. (**d**) Schematic illustration of the hybrid generation system[129]. (**e**) Schematic illustration (left), and electron energy band diagram of the PSC-TE hybrid device[130]. (**f**) Schematic cross section of ZnO nanowires/CIGS solar cell connected to the thermoelectric generator[131]. (**g**) Schematic illustration of the photovoltaic-thermoelectric hybrid device (left), and best performed J-V curves (symbol-line) and output power (dash-line) of the PSC/TE hybrid devices tested with the assisted cooling system or not (right)[132]. ref.[132], Copyright © 2017 Elsevier. (**h**) Non-contact reflection geometry (left), non-contact transmission geometry (middle), and contact transmission geometry (right)[134]. (**i**) Calculated TEG efficiencies for the PV-TEG hybrid system in the three different geometries[134]. Figure reproduced with permission from: (a) ref.[128], Copyright © 2014 Elsevier; (b, c) ref.[127], Copyright © 2012 Elsevier; (d) ref.[129], Copyright © 2013 Elsevier; (e) ref.[130], Copyright © 2018 John Wiley and Sons; (f) ref.[131], Copyright © 2015 John Wiley and Sons; (g–i) ref.[134], Copyright © 2021 Royal Society of Chemistry.

work, the effect of geometry on the total energy conversion efficiency in the SC-TEG hybrid system was studied (Fig. 8(h)). Their work involved three different geometries: reflection, non-contact, and contact transmission geometries. Figure 8(i) shows that the contact transmission geometry could produce the highest temperature differences for the TEG module, resulting in the most efficient energy conversion for the SC-TEG hybrid system.

Summary and perspectives

The recent research results of the SCHEH based on TENG, PENG, and TEG are described in this brief review. Compared to other reported HEHs such as triboelectric-piezoelectric HEHs, triboelectric-electromagnetic HEHs, or triboelectric-thermoelectric HEHs, the introduction of SCs in SCHEHs provides the hybrid systems with higher DC output currents which are more in line with the requirements of current electrical devices. Meanwhile, solar energy is the most promising energy source for human beings owing to its abundance in reserves, cleanness in usage, and universality in regions. The pros and cons of the different SCHEHs are summarized in Table 1. Besides the introduced TENG, PENG, and TEG, EMG and pyroelectric nanogenerator (PyNG) are the other two typical energy harvesting technology units to be adopted as supplements for fabricating SCHEHs[135,136]. Further development of the SCHEH technology could result from the introduction of a third or even fourth energy harvesting or storage technology into the hybrid system. For instance, Shao et al. proposed a multifunctional power unit by hybridizing TENG, EMG, and solar cell[137]. In their multifunctional system, the TENG module enabled to harvest lower-frequency (<0.5 Hz) mechanical motions, while the EMG module could collect energy from mechanical movements at relatively high-frequency. Triggered by the mechanical energy from water waves at 2 Hz, the TENG module could produce an output voltage of 142 V and an output current of 23.3 μA. For the EMG module, an output voltage of 0.66 V and an output current of 2.14 mA could be attained. With the further integration of a water-proof Si-based solar cell module, this multifunctional system achieved the purpose of harvesting energy in a broader way. In 2012, Yang and coauthors fabricated the first flexible SCHEHs based on solar cell, PENG, and PyNG for simultaneously harvesting solar, mechanical, and thermal energies[138]. With both pyroelectric and piezoelectric properties, the fabricated flexible SCHEHs could drive an LCD by using the hand-touching-induced hybrid thermal and mechanical energies. Finally, the whole generated electricity could be stored in a Li-ion battery for lighting four LEDs in parallel connection. Moreover, it needs to be emphasized that the synergetic effect of hybridizing solar cells with other energy harvesters entails achieving enhanced performance and overall energy generation by integrating different energy harvesting technologies into a single system. By integrating solar cells with other energy harvesters, the hybrid system can harvest energy from multiple sources simultaneously. This integration enables the system to maximize the overall energy generation. Solar cells primarily rely on sunlight for energy generation, which can be influenced by factors like shading, weather conditions, or limited exposure to direct sunlight. Through integration, the hybrid system can complement solar energy with energy from alternative sources. Thus, even when sunlight is unavailable or insufficient, the other energy harvesters can continue to generate electricity from mechanical vibrations, temperature differentials, or other ambient sources. This complementary approach ensures a more consistent and reliable energy supply. We know each energy harvesting technology presents distinct strengths and limitations in terms of energy conversion efficiency for specific sources. The hybrid system can leverage the unique properties and conversion capabilities of each component. For instance, the solar cells excel in converting sunlight into electricity, while the PENG demonstrates

Table 1 | Comparison of the different types of SCHEHs.

	Pros	Cons
SC-TENG	High output voltage long lifetime low cost Easy fabrication Wide-frequency bandwidth	High impedance Low output current
SC-PENG	Tight integration Low weight Simple structure	Low output power and current Lab-scale applications High efficiency in high-frequency
SC-TEG	High output power and current Wide compatibility DC outputs No external mechanical energy sources needed (natural heat generation)	Low output voltage Structure complexity Weather limitations

efficiency in converting high-frequency mechanical vibrations into electrical energy. By employing the most suitable technology for each energy source, the hybrid system optimizes energy conversion, resulting in enhanced overall efficiency and performance. Additionally, the hybrid design enhances power density by integrating multiple energy harvesting technologies into a compact system, which is particularly advantageous in practical applications with space constraints, such as wearable devices or small-scale electronics. Furthermore, in case of one component encounters limitations or temporarily produces lower energy output, the others can compensate and maintain a continuous power generation.

Overall, SCHEHs present a highly promising approach to optimize energy conversion and enhance the versatility of energy harvesting systems. By integrating the advantages of solar cell technology with various other energy harvesting techniques, these systems make significant contributions to sustainable and efficient power generation in diverse applications, for example, a hybrid system has been considered a promising solution in self-powered systems, remote monitoring, and smart transport applications[1]. Moreover, they also play a key role in supporting the ongoing transition towards a more renewable energy future. However, the current challenges are that increasing the efficiency by a significant margin cannot be achieved in a short period of time[139]. Thus, future directions should be oriented towards i) enhancing the efficiency of the hybrid system and ii) improving the cost performance. Furthermore, each module of the SCHEH hybrid system has different characteristics of the underlying working principles, output voltages and output currents. Therefore, it is essential to design a more effective power-management integrated circuit, which is suitable for the SCHEH to improve the energy conversion and storage efficiency of the whole hybrid system. In addition to improving their power density, miniaturization of the device current is also important for certain applications such as wearable electronics or implantable devices.

References

1. Pang YK, Cao YT, Derakhshani M, Fang YH, Wang ZL et al. Hybrid energy-harvesting systems based on triboelectric nanogenerators. *Matter* **4**, 116–143 (2021).
2. Zhong JW, Zhong QZ, Hu QY, Wu N, Li WB et al. Stretchable self‐powered fiber‐based strain sensor. *Adv Funct Mater* **25**, 1798–1803 (2015).
3. Xu CH, Yang YR, Gao W. Skin-interfaced sensors in digital medicine: from materials to applications. *Matter* **2** 1414–1445 (2020).
4. Salter SH. Wave power. *Nature* **249**, 720–724 (1974).
5. Liang SZ, Wang XY, Cheng YJ, Xia YG, Müller-Buschbaum P. Anatase titanium dioxide as rechargeable ion battery electrode-a chronological review. *Energy Storage Mater* **45**, 201–264 (2022).
6. Herbert GMJ, Iniyan S, Sreevalsan E, Rajapandian S. A review of wind energy technologies. *Renew Sustainable Energy Rev* **11**, 1117–1145 (2007).
7. Lehmann J. Bio‐energy in the black. *Front Ecol Environ* **5**, 381–387 (2007).
8. Lai YC, Hsiao YC, Wu HM, Wang ZL. Waterproof fabric‐based multifunctional triboelectric nanogenerator for universally harvesting energy from raindrops, wind, and human motions and as self‐powered sensors. *Adv Sci* **6**, 1801883 (2019).
9. Cho Y, Lee K, Park S, Ahn S, Kim W et al. Rotational wind power triboelectric nanogenerator using aerodynamic changes of friction area and the adsorption effect of hematoxylin onto feather based on a diversely evolved hyper-branched structure. *Nano Energy* **61**, 370–380 (2019).
10. Elbanna A, Chaykun K, Lekina Y, Liu YD, Febriansyah B et al. Perovskite-transition metal dichalcogenides heterostructures: recent advances and future perspectives. *Opto-Electron Sci* **1**, 220006 (2022).
11. Tan DZ, Sun K, Li ZL, Xu BB, Qiu JR. Photo-processing of perovskites: current research status and challenges. *Opto-Electron Sci* **1**, 220014 (2022).
12. Jiang XY, Chotard P, Luo KX, Eckmann F, Tu S et al. Revealing donor-acceptor interaction on the printed active layer morphology and the formation kinetics for nonfullerene organic solar cells at ambient conditions. *Adv Energy Mater* **12**, 2103977 (2022).
13. Zou YQ, Yuan S, Buyruk A, Eichhorn J, Yin SS et al. The influence of CsBr on crystal orientation and optoelectronic properties of $MAPbI_3$-based solar cells. *ACS Appl Mater Interfaces* **14**, 2958–2967 (2022).
14. Yang Y, Chen L, He J, Hou XJ, Qiao XJ et al. Flexible and extendable honeycomb‐shaped triboelectric nanogenerator for effective human motion energy harvesting and biomechanical sensing. *Adv Mater Technol* **7**, 2100702 (2022).
15. Guo TM, Gong YJ, Li ZG, Liu YM, Li W et al. A new hybrid lead‐free metal halide piezoelectric for energy harvesting and human motion sensing. *Small* **18**, 2103829 (2022).
16. Qu XC, Liu Z, Tan PC, Wang C, Liu Y et al. Artificial tactile perception smart finger for material identification based on triboelectric sensing. *Sci Adv* **8**, eabq2521 (2022).
17. Jiang DJ, Shi BJ, Ouyang H, Fan YB, Wang ZL et al. Emerging implantable energy harvesters and self-powered implantable medical electronics. *ACS Nano* **14**, 6436–6448 (2020).
18. Guo XG, He TYY, Zhang ZX, Luo AX, Wang F et al. Artificial intelligence-enabled caregiving walking stick powered by ultra-low-frequency human motion. *ACS Nano* **15**, 19054–19069 (2021).
19. Xiao TX, Jiang T, Zhu JX, Liang X, Xu L et al. Silicone-based triboelectric nanogenerator for water wave energy harvesting. *ACS Appl Mater Interfaces* **10**, 3616–3623 (2018).
20. Liang X, Jiang T, Liu GX, Feng YW, Zhang C et al. Spherical triboelectric nanogenerator integrated with power manage-

ment module for harvesting multidirectional water wave energy. *Energy Environ Sci* **13**, 277–285 (2020).
21. Jiang T, Pang H, An J, Lu PJ, Feng YW et al. Robust swing‐structured triboelectric nanogenerator for efficient blue energy harvesting. *Adv Energy Mater* **10**, 2000064 (2020).
22. Cheng C, Dai YW, Yu J, Liu C, Wang SJ et al. Review of liquid-based systems to recover low-grade waste heat for electrical energy generation. *Energy Fuels* **35**, 161–175 (2021).
23. Bell LE. Cooling, heating, generating power, and recovering waste heat with thermoelectric systems. *Science* **321**, 1457–1461 (2008).
24. Lee TD, Ebong AU. A review of thin film solar cell technologies and challenges. *Renew Sustainable Energy Rev* **70**, 1286–1297 (2017).
25. Sengupta D, Das P, Mondal B, Mukherjee K. Effects of doping, morphology and film-thickness of photo-anode materials for dye sensitized solar cell application-a review. *Renew Sustainable Energy Rev* **60**, 356–376 (2016).
26. Sathiyan G, Sivakumar EKT, Ganesamoorthy R, Thangamuthu R, Sakthivel P. Review of carbazole based conjugated molecules for highly efficient organic solar cell application. *Tetrahedron Lett* **57**, 243–252 (2016).
27. Kim JY, Lee JW, Jung HS, Shin H, Park NG. High-efficiency perovskite solar cells. *Chem Rev* **120**, 7867–7918 (2020).
28. Wu TH, Qin ZZ, Wang YB, Wu YZ, Chen W et al. The main progress of perovskite solar cells in 2020-2021. *Nano-Micro Lett* **13**, 152 (2021).
29. Xie L, Song W, Ge JF, Tang BC, Zhang XL et al. Recent progress of organic photovoltaics for indoor energy harvesting. *Nano Energy* **82**, 105770 (2021).
30. Cui Y, Yao HF, Hong L, Zhang T, Tang YB et al. Organic photovoltaic cell with 17% efficiency and superior processability. *Natl Sci Rev* **7**, 1239–1246 (2020).
31. Dréon J, Jeangros Q, Cattin J, Haschke J, Antognini L et al. 23.5%-efficient silicon heterojunction silicon solar cell using molybdenum oxide as hole-selective contact. *Nano Energy* **70**, 104495 (2020).
32. Nayak PK, Mahesh S, Snaith HJ, Cahen D. Photovoltaic solar cell technologies: analysing the state of the art. *Nat Rev Mater* **4**, 269–285 (2019).
33. Yuan JY, Hazarika A, Zhao Q, Ling XF, Moot T et al. Metal halide perovskites in quantum dot solar cells: progress and prospects. *Joule* **4**, 1160–1185 (2020).
34. Hu L, Zhao Q, Huang SJ, Zheng JH, Guan XW et al. Flexible and efficient perovskite quantum dot solar cells via hybrid interfacial architecture. *Nat Commun* **12**, 466 (2021).
35. Chen D, Vaqueiro Contreras M, Ciesla A, Hamer P, Hallam B et al. Progress in the understanding of light‐ and elevated temperature‐induced degradation in silicon solar cells: a review. *Prog Photovolt Res Appl* **29**, 1180–1201 (2021).
36. Omazic A, Oreski G, Halwachs M, Eder GC, Hirschl C et al. Relation between degradation of polymeric components in crystalline silicon PV module and climatic conditions: a literature review. *Sol Energy Mater Sol Cells* **192**, 123–133 (2019).
37. Dunfield SP, Bliss L, Zhang F, Luther JM, Zhu K et al. From defects to degradation: a mechanistic understanding of degradation in perovskite solar cell devices and modules. *Adv Energy Mater* **10**, 1904054 (2020).
38. Kundu S, Kelly TL. In situ studies of the degradation mechanisms of perovskite solar cells. *EcoMat* **2**, e12025 (2020).
39. Guo RJ, Han D, Chen W, Dai LJ, Ji KY et al. Degradation mechanisms of perovskite solar cells under vacuum and one atmosphere of nitrogen. *Nat Energy* **6**, 977–986 (2021).
40. Xiong Z, Chen X, Zhang B, Odunmbaku GO, Ou ZP et al. Simultaneous interfacial modification and crystallization control by biguanide hydrochloride for stable perovskite solar cells with PCE of 24.4%. *Adv Mater* **34**, 2106118 (2022).
41. Sharma R, Sharma A, Agarwal S, Dhaka MS. Stability and efficiency issues, solutions and advancements in perovskite solar cells: a review. *Sol Energy* **244**, 516–535 (2022).
42. Li CQ, Gu XB, Chen ZH, Han X, Yu N et al. Achieving record-efficiency organic solar cells upon tuning the conformation of solid additives. *J Am Chem Soc* **144**, 14731–14739 (2022).
43. Tang QW. All‐weather solar cells: a rising photovoltaic revolution. *Chem Eur J* **23**, 8118–8127 (2017).
44. Ryu H, Yoon HJ, Kim SW. Hybrid energy harvesters: toward sustainable energy harvesting. *Adv Mater* **31**, 1802898 (2019).
45. Wu YH, Qu JK, Chu PK, Shin DM, Luo Y et al. Hybrid photovoltaic-triboelectric nanogenerators for simultaneously harvesting solar and mechanical energies. *Nano Energy* **89**, 106376 (2021).
46. Gautam A, Saini RP. A review on technical, applications and economic aspect of packed bed solar thermal energy storage system. *J Energy Storage* **27**, 101046 (2020).
47. Makki A, Omer S, Sabir H. Advancements in hybrid photovoltaic systems for enhanced solar cells performance. *Renew Sustainable Energy Rev* **41**, 658–684 (2015).
48. Yang Y, Wang ZL. Hybrid energy cells for simultaneously harvesting multi-types of energies. *Nano Energy* **14**, 245–256 (2015).
49. Fan FR, Tian ZQ, Wang ZL. Flexible triboelectric generator. *Nano Energy* **1**, 328–334 (2012).
50. Yang YQ, Guo XG, Zhu ML, Sun ZD, Zhang ZX et al. Triboelectric nanogenerator enabled wearable sensors and electronics for sustainable internet of things integrated green earth. *Adv Energy Mater* **13**, 2203040 (2023).
51. Wang ZL, Song JH. Piezoelectric nanogenerators based on zinc oxide nanowire arrays. *Science* **312**, 242–246 (2006).
52. Champier D. Thermoelectric generators: a review of applications. *Energy Convers Manag* **140**, 167–181 (2017).
53. Sivasubramanian R, Vaithilingam CA, Indira SS, Paiman S, Misron N et al. A review on photovoltaic and nanogenerator hybrid system. *Mater Today Energy* **20**, 100772 (2021).
54. Das D, Kalita P, Roy O. Flat plate hybrid photovoltaic-thermal (PV/T) system: a review on design and development. *Renew Sustainable Energy Rev* **84**, 111–130 (2018).
55. Wang J, Xiao F, Zhao H. Thermoelectric, piezoelectric and photovoltaic harvesting technologies for pavement engineering. *Renew Sustainable Energy Rev* **151**, 111522 (2021).
56. Sharov VA, Alekseev PA, Borodin BR, Dunaevskiy MS, Reznik RR et al. InP/Si heterostructure for high-current hybrid triboelectric/photovoltaic generation. *ACS Appl Energy Mater* **2**, 4395–4401 (2019).
57. Bensmail S, Rekioua D, Azzi H. Study of hybrid photovoltaic/fuel cell system for stand-alone applications. *Int J Hydrogen Energy* **40**, 13820–13826 (2015).
58. Chen YD, Jie Y, Zhu JQ, Lu QX, Cheng Y et al. Hybridized triboelectric-electromagnetic nanogenerators and solar cell for energy harvesting and wireless power transmission. *Nano Res* **15**, 2069–2076 (2022).

59. Cao R, Wang JN, Xing Y, Song WX, Li NW et al. A self-powered lantern based on a triboelectric-photovoltaic hybrid nanogenerator. *Adv Mater* **3**, 1700371 (2018).
60. Le XH, Guo XG, Lee C. Evolution of micro-nano energy harvesting technology—scavenging energy from diverse sources towards self-sustained micro/nano systems. *Nanoenergy Adv* **3**, 101–125 (2023).
61. Qiu CK, Wu F, Lee C, Yuce MR. Self-powered control interface based on gray code with hybrid triboelectric and photovoltaics energy harvesting for IoT smart home and access control applications. *Nano Energy* **70**, 104456 (2020).
62. Luque A, Hegedus S. *Handbook of Photovoltaic Science and Engineering* 2nd ed (Wiley, Chichester, 2011).
63. Halme J, Vahermaa P, Miettunen K, Lund P. Device physics of dye solar cells. *Adv Mater* **22**, E210–E234 (2010).
64. Clarke TM, Durrant JR. Charge photogeneration in organic solar cells. *Chem Rev* **110**, 6736–6767 (2010).
65. Li H, Zhou JJ, Tan LG, Li MH, Jiang CF et al. Sequential vacuum-evaporated perovskite solar cells with more than 24% efficiency. *Sci Adv* **8**, eabo7422 (2022).
66. Sun YN, Chang MJ, Meng LX, Wan XJ, Gao HH et al. Flexible organic photovoltaics based on water-processed silver nanowire electrodes. *Nat Electron* **2**, 513–520 (2019).
67. Yang ZY, Fan JZ, Proppe AH, Arquer FPGD, Rossouw D et al. Mixed-quantum-dot solar cells. *Nat Commun* **8**, 1325 (2017).
68. Rath AK, Bernechea M, Martinez L, De Arquer FPG, Osmond J et al. Solution-processed inorganic bulk nano-heterojunctions and their application to solar cells. *Nat Photonics* **6**, 529–534 (2012).
69. Luo X, Luo HW, Li HJ, Xia R, Zheng XT et al. Efficient perovskite/silicon tandem solar cells on industrially compatible textured silicon. *Adv Mater* **35**, 2207883 (2023).
70. Reb LK, Böhmer M, Predeschly B, Grott S, Weindl CL et al. Perovskite and organic solar cells on a rocket flight. *Joule* **4**, 1880–1892 (2020).
71. Wang ZL, Wang AC. On the origin of contact-electrification. *Mater Today* **30**, 34–51 (2019).
72. Wang ZL. On Maxwell's displacement current for energy and sensors: the origin of nanogenerators. *Mater Today* **20**, 74–82 (2017).
73. Kim S, Gupta MK, Lee KY, Sohn A, Kim TY et al. Transparent flexible graphene triboelectric nanogenerators. *Adv Mater* **26**, 3918–3925 (2014).
74. Saha CR, O'Donnell T, Wang N, McCloskey P. Electromagnetic generator for harvesting energy from human motion. *Sens Actuators A Phys* **147**, 248–253 (2008).
75. Zhao JQ, Zhen GW, Liu GX, Bu TZ, Liu WB et al. Remarkable merits of triboelectric nanogenerator than electromagnetic generator for harvesting small-amplitude mechanical energy. *Nano Energy* **61**, 111–118 (2019).
76. Hinchet R, Yoon HJ, Ryu H, Kim MK, Choi EK et al. Transcutaneous ultrasound energy harvesting using capacitive triboelectric technology. *Science* **365**, 491–494 (2019).
77. Zi YL, Wang ZL. Nanogenerators: an emerging technology towards nanoenergy. *APL Mater* **5**, 074103 (2017).
78. Zhao ZF, Pu X, Du CH, Li LX, Jiang CY et al. Freestanding flag-type triboelectric nanogenerator for harvesting high-altitude wind energy from arbitrary directions. *ACS Nano* **10**, 1780–1787 (2016).
79. Xiao TX, Liang X, Jiang T, Xu L, Shao JJ et al. Spherical triboelectric nanogenerators based on spring‐assisted multilayered structure for efficient water wave energy harvesting. *Adv Funct Mater* **28**, 1802634 (2018).
80. Kang Y, Wang B, Dai SG, Liu GL, Pu YP et al. Folded elastic strip-based triboelectric nanogenerator for harvesting human motion energy for multiple applications. *ACS Appl Mater Interfaces* **7**, 20469–20476 (2015).
81. Huang T, Wang C, Yu H, Wang HZ, Zhang QH et al. Human walking-driven wearable all-fiber triboelectric nanogenerator containing electrospun polyvinylidene fluoride piezoelectric nanofibers. *Nano Energy* **14**, 226–235 (2015).
82. Wang C, Hu YR, Liu Y, Shan YZ, Qu XC et al. Tissue‐adhesive piezoelectric soft sensor for in vivo blood pressure monitoring during surgical operation. *Adv Funct Mater* , 202303696 (2023).
83. Qin Y, Wang XD, Wang ZL. Microfibre-nanowire hybrid structure for energy scavenging. *Nature* **451**, 809–813 (2008).
84. Zhang C, Fan W, Wang SJ, Wang Q, Zhang YF et al. Recent progress of wearable piezoelectric nanogenerators. *ACS Appl Electron Mater* **3**, 2449–2467 (2021).
85. Xu S, Qin Y, Xu C, Wei YG, Yang RS et al. Self-powered nanowire devices. *Nat Nanotechnol* **5**, 366–373 (2010).
86. Park KI, Son JH, Hwang GT, Jeong CK, Ryu J et al. Highly‐efficient, flexible piezoelectric PZT thin film nanogenerator on plastic substrates. *Adv Mater* **26**, 2514–2520 (2014).
87. Zhang M, Gao T, Wang JS, Liao JJ, Qiu YQ et al. Single BaTiO_3 nanowires-polymer fiber based nanogenerator. *Nano Enery* **11**, 510–517 (2015).
88. Chang C, Tran VH, Wang JB, Fuh YK, Lin LW. Direct-write piezoelectric polymeric nanogenerator with high energy conversion efficiency. *Nano Lett* **10**, 726–731 (2010).
89. Zhang X, Chen JF, Wang Y. Hierarchical $PbZr_xTi_{1-x}O_3$ nanowires for vibrational energy harvesting. *ACS Appl Nano Mater* **1**, 1461–1466 (2018).
90. Shi XL, Zou J, Chen ZG. Advanced thermoelectric design: from materials and structures to devices. *Chem Rev* **120**, 7399–7515 (2020).
91. Yang L, Chen ZG, Dargusch MS, Zou J. High performance thermoelectric materials: progress and their applications. *Adv Energy Mater* **8**, 1701797 (2018).
92. Oechsle AL, Heger JE, Li N, Yin SS, Bernstorff S et al. Correlation of thermoelectric performance, domain morphology and doping level in PEDOT: PSS thin films post‐treated with ionic liquids. *Macromol Rapid Commun* **42**, 2100397 (2021).
93. Tu S, Tian T, Oechsle AL, Yin SS, Jiang XY et al. Improvement of the thermoelectric properties of PEDOT: PSS films via DMSO addition and DMSO/salt post-treatment resolved from a fundamental view. *Chem Eng J* **429**, 132295 (2022).
94. Xie WJ, Weidenkaff A, Tang XF, Zhang QJ, Poon J et al. Recent advances in nanostructured thermoelectric half-Heusler compounds. *Nanomaterials* **2**, 379–412 (2012).
95. Liu ZJ, Tian B, Li Y, Lei JM, Zhang ZK et al. A large-area bionic skin for high-temperature energy harvesting applications. *Nano Res* **16**, 10245–10255 (2023).
96. Migita T, Tachikawa N, Katayama Y, Miura T. Thermoelectromotive force of some redox couples in an amide-type room-temperature ionic liquid. *Electrochemistry* **77**, 639–641 (2009).
97. Orr B, Akbarzadeh A, Mochizuki M, Singh R. A review of car waste heat recovery systems utilising thermoelectric generators and heat pipes. *Appl Therm Eng* **101**, 490–495 (2016).

98. Iezzi B, Ankireddy K, Twiddy J, Losego MD, Jur JS. Printed, metallic thermoelectric generators integrated with pipe insulation for powering wireless sensors. *Appl Energy* **208**, 758–765 (2017).
99. Proto A, Penhaker M, Conforto S, Schmid M. Nanogenerators for human body energy harvesting. *Trends Biotechnol* **35**, 610–624 (2017).
100. Settaluri KT, Lo H, Ram RJ. Thin thermoelectric generator system for body energy harvesting. *J Electron Mater* **41**, 984–988 (2012).
101. Trung NH, Van Toan N, Ono T. Flexible thermoelectric power generator with Y-type structure using electrochemical deposition process. *Appl Energy* **210**, 467–476 (2018).
102. Russ B, Glaudell A, Urban JJ, Chabinyc ML, Segalman RA. Organic thermoelectric materials for energy harvesting and temperature control. *Nat Rev Mater* **1**, 16050 (2016).
103. Zhang FJ, Zang YP, Huang DZ, Di CA, Zhu DB. Flexible and self-powered temperature-pressure dual-parameter sensors using microstructure-frame-supported organic thermoelectric materials. *Nat Commun* **6**, 8356 (2015).
104. Shi H, Liu CC, Jiang QL, Xu JK. Effective approaches to improve the electrical conductivity of PEDOT: PSS: a review. *Adv Electron Mater* **1**, 1500017 (2015).
105. Bießmann L, Kreuzer LP, Widmann T, Hohn N, Moulin JF et al. Monitoring the swelling behavior of PEDOT: PSS electrodes under high humidity conditions. *ACS Appl Mater Interfaces* **10**, 9865–9872 (2018).
106. Palumbiny CM, Liu F, Russell TP, Hexemer A, Wang C et al. The crystallization of PEDOT: PSS polymeric electrodes probed in situ during printing. *Adv Mater* **27**, 3391–3397 (2015).
107. Oechsle AL, Heger JE, Li N, Yin SS, Bernstorff S et al. *In situ* observation of morphological and oxidation level degradation processes within ionic liquid post-treated PEDOT: PSS thin films upon operation at high temperatures. *ACS Appl Mater Interfaces* **14**, 30802–30811 (2022).
108. Saxena N, Pretzl B, Lamprecht X, Bießmann L, Yang D et al. Ionic liquids as post-treatment agents for simultaneous improvement of Seebeck coefficient and electrical conductivity in PEDOT: PSS Films. *ACS Appl Mater Interfaces* **11**, 8060–8071 (2019).
109. Kluge RM, Saxena N, Chen W, Körstgens V, Schwartzkopf M et al. Doping dependent in‐plane and cross‐plane thermoelectric performance of thin n‐type polymer P(NDI2OD‐T2) films. *Adv Funct Mater* **30**, 2003092 (2020).
110. Kluge RM, Saxena N, Müller-Buschbaum, P. A solution-processable polymer-based thin-film thermoelectric generator. *Adv Energy Sustainability Res* **2**, 2000060 (2021).
111. Huo ZY, Lee DM, Kim YJ, Kim SW. Solar-induced hybrid energy harvesters for advanced oxidation water treatment. *IScience* **24**, 102808 (2021).
112. Liu YQ, Sun N, Liu JW, Wen Z, Sun XH et al. Integrating a silicon solar cell with a triboelectric nanogenerator *via* a mutual electrode for harvesting energy from sunlight and raindrops. *ACS Nano* **12**, 2893–2899 (2018).
113. Zhao LL, Duan JL, Liu LQ, Wang JW, Duan YY et al. Boosting power conversion efficiency by hybrid triboelectric nanogenerator/silicon tandem solar cell toward rain energy harvesting. *Nano Energy* **82**, 105773 (2021).
114. Ren ZY, Zheng Q, Wang HB, Guo H, Miao LM et al. Wearable and self-cleaning hybrid energy harvesting system based on micro/nanostructured haze film. *Nano Energy* **67**, 104243 (2020).
115. Pu X, Song WX, Liu MM, Sun CW, Du CH et al. Wearable power‐textiles by integrating fabric triboelectric nanogenerators and fiber‐shaped dye‐sensitized solar cells. *Adv Energy Mater* **6**, 1601048 (2016).
116. Kim B, Song JY, Kim DY, Kim MC, Lin ZH et al. All-aerosol-sprayed high-performance transparent triboelectric nanogenerator with embedded charge-storage layer for self-powered invisible security IoT system and raindrop-solar hybrid energy harvester. *Nano Energy* **104**, 107878 (2022).
117. Liu T, Zheng Y, Xu YX, Liu XJ, Wang CF et al. Semitransparent polymer solar cell/triboelectric nanogenerator hybrid systems: Synergistic solar and raindrop energy conversion for window-integrated applications. *Nano Energy* **103**, 107776 (2022).
118. Liu YQ, Li EL, Yan YJ, Lin ZN, Chen QZ et al. A one-structure-layer PDMS/Mxenes based stretchable triboelectric nanogenerator for simultaneously harvesting mechanical and light energy. *Nano Energy* **86**, 106118 (2021).
119. Xu C, Wang XD, Wang ZL. Nanowire structured hybrid cell for concurrently scavenging solar and mechanical energies. *J Am Chem Soc* **131**, 5866–5872 (2009).
120. Xu C, Wang ZL. Compact hybrid cell based on a convoluted nanowire structure for harvesting solar and mechanical energy. *Adv Mater* **23**, 873–877 (2011).
121. Ahmed R, Kim Y, Zeeshan, Chun W. Development of a tree-shaped hybrid nanogenerator using flexible sheets of photovoltaic and piezoelectric films. *Energies* **12**, 229 (2019).
122. Yoon GC, Shin KS, Gupta MK, Lee KY, Lee JH et al. High-performance hybrid cell based on an organic photovoltaic device and a direct current piezoelectric nanogenerator. *Nano Energy* **12**, 547–555 (2015).
123. Liu X, Li J, Fang ZZ, Wang C, Shu LS et al. Ultraviolet-protecting, flexible and stable photovoltaic-assisted piezoelectric hybrid unit nanogenerator for simultaneously harvesting ultraviolet light and mechanical energies. *J Mater Sci* **55**, 15222–15237 (2020).
124. Kim YM, Kim W, Choi DW, Choi DH. Reliable output performance of a photovoltaic–piezoelectric hybridized energy harvester with an automatic position-adjustable bending instrument. *Int. J Precis Eng Manuf - Green Technol* **9**, 1077–1086 (2022).
125. Lee DH. Direct parallel and hybrid power control scheme of a low-power PV and piezoelectric energy harvesting module. *J Electr Eng Technol* **16**, 2045–2053 (2021).
126. Sundarraj P, Maity D, Roy SS, Taylor RA. Recent advances in thermoelectric materials and solar thermoelectric generators-a critical review. *RSC Adv* **4**, 46860–46874 (2014).
127. Ju X, Wang ZF, Flamant G, Li P, Zhao WY. Numerical analysis and optimization of a spectrum splitting concentration photovoltaic-thermoelectric hybrid system. *Sol Energy* **86**, 1941–1954 (2012).
128. Li YL, Witharana S, Cao H, Lasfargues M, Huang Y et al. Wide spectrum solar energy harvesting through an integrated photovoltaic and thermoelectric system. *Particuology* **15**, 39–44 (2014).
129. Deng Y, Zhu W, Wang Y, Shi YM. Enhanced performance of solar-driven photovoltaic-thermoelectric hybrid system in an in-

tegrated design. *Sol Energy* **88**, 182–191 (2013).
130. Xu L, Xiong Y, Mei AY, Hu Y, Rong YG et al. Efficient perovskite photovoltaic - thermoelectric hybrid device. *Adv Energy Mater* **8**, 1702937 (2018).
131. Hsueh TJ, Shieh JM, Yeh YM. Hybrid Cd - free CIGS solar cell/TEG device with ZnO nanowires. *Prog Photovolt Res Appl* **23**, 507–512 (2015).
132. Liu ZY, Sun B, Zhong Y, Liu XY, Han JH et al. Novel integration of carbon counter electrode based perovskite solar cell with thermoelectric generator for efficient solar energy conversion. *Nano Energy* **38**, 457–466 (2017).
133. Zhou YP, He YL, Qiu Y, Ren QL, Xie T. Multi-scale investigation on the absorbed irradiance distribution of the nanostructured front surface of the concentrated PV-TE device by a MC-FDTD coupled method. *Appl Energy* **207**, 18–26 (2017).
134. Jurado JP, Dörling B, Zapata-Arteaga O, Goñi AR, Campoy-Quiles M. Comparing different geometries for photovoltaic-thermoelectric hybrid devices based on organics. *J Mater Chem C* **9**, 2123–2132 (2021).
135. Zhang KW, Wang YH, Yang Y. Structure design and performance of hybridized nanogenerators. *Adv Funct Mater* **29**, 1806435 (2019).
136. Zhang KW, Wang ZL, Yang Y. Enhanced P3HT/ZnO nanowire array solar cells by pyro-phototronic effect. *ACS Nano* **10**, 10331–10338 (2016).
137. Shao HY, Wen Z, Cheng P, Sun N, Shen QQ et al. Multifunctional power unit by hybridizing contact-separate triboelectric nanogenerator, electromagnetic generator and solar cell for harvesting blue energy. *Nano Energy* **39**, 608–615 (2017).
138. Yang Y, Zhang HL, Zhu G, Lee S, Lin ZH et al. Flexible hybrid energy cell for simultaneously harvesting thermal, mechanical, and solar energies. *ACS Nano* **7**, 785–790 (2013).
139. Yoon HJ, Kwak SS, Kim SM, Kim SW. Aim high energy conversion efficiency in triboelectric nanogenerators. *Sci Technol Adv Mater* **21**, 683–688 (2020).

Acknowledgements

We are grateful for financial support from the Deutsche Forschungsgemeinschaft (DFG, German Research Foundation) via Germany's Excellence Strategy-EXC 2089/1-390776260 (e-conversion) and via the International Research Training Group 2022 the Alberta/Technical University of Munich International Graduate School for Environmentally Responsible Functional Materials (ATUMS), TUM.solar in the context of the Bavarian Collaborative Research Project Solar Technologies Go Hybrid (SolTech), the Center for NanoScience (CeNS), and the China Scholarship Council (CSC).

Author contributions

TX Xiao and S Tu contributed equally to this work and drafted the manuscript. TX Xiao and SZ Liang provided visualizations. RJ Guo contributed to the part on solar cells. T Tian contributed to the part on thermoelectric generators. P Müller-Buschbaum supervised the review. All authors read, corrected and approved the manuscript.

Competing interests

The authors declare no competing financial interests.